

R-08-30

Thermo-mechanical analyses of a KBS-3H deposition drift at Olkiluoto site

Margareta Lönnqvist, Harald Hökmark
Clay Technology AB

December 2008

Svensk Kärnbränslehantering AB

Swedish Nuclear Fuel
and Waste Management Co

Box 250, SE-101 24 Stockholm
Phone +46 8 459 84 00



ISSN 1402-3091

SKB Rapport R-08-30

Thermo-mechanical analyses of a KBS-3H deposition drift at Olkiluoto site

Margareta Lönnqvist, Harald Hökmark
Clay Technology AB

December 2008

Keywords: Thermal stresses, Rock spalling, T-M model, T-M analyses, Rock failure, KBS-3H.

This report is a result of a joint project between SKB and Posiva. This report is also printed as a Posiva WR report, Posiva WR 2007-66.

A pdf version of this document can be downloaded from www.skb.se.

Abstract

The stresses on the perimeter of a KBS-3H deposition drift at Olkiluoto site, specifically occurrence of spalling in roof and floor areas and opening of joints intersecting the deposition drifts horizontally at mid-height have been evaluated.

The effects different *in situ* stress orientations and magnitudes have on drift perimeter stresses due to excavation and heating have been evaluated.

Swelling buffer materials and the build up of gas within the deposition drifts will exert a pressure on the drift walls. The pressures needed to open a horizontally intersecting joint at specific points in time and the resulting increase in aperture have also been evaluated.

The key results of the study indicate that significant spalling after excavation is not likely to occur for the reference layout, *i.e.* with deposition drifts being parallel or sub-parallel to the major *in situ* stress. The spalling stability margin is of the order of 15–30 MPa, taking laboratory-determined values of the crack initiation stress σ_{CI} as a measure of the spalling strength. It should be noted, however, that results from the APSE field experiment at Äspö HRL and from the Mine-by Experiment at AECL's URL indicate that the spalling strength probably is larger in reality. /Martin 2005/ suggests, based on observations from these experiments, that the spalling strength corresponds to 57% of the laboratory-determined uniaxial compressive strength. This means that the spalling risk estimates made here are well on the conservative side. However, without any support pressure on the drift periphery induced by e.g. swelling of buffer, spalling is almost certain to occur in the roof and floor regions after a few years of heating, irrespective of how drifts are oriented in relation to the *in situ* stresses. This is true for drift sections at canister mid-length as well as sections between canister positions. After 50 years the thermal stress additions alone are found to exceed the spalling strength by approximately 20 MPa. At that time, the total roof and floor stresses may even be on level or close to the uniaxial compressive strength (UCS) reported for the dominating rock type.

To open a horizontal fracture intersecting the un-heated drift at mid-height (*i.e.* increasing the undisturbed pre-mining aperture) requires drift pressures of the order of 10 MPa are required in the deposition drift. To open it sufficiently to bring the fracture into tension at distances between 0 m and 0.2 m from the periphery requires about 20 to 25 MPa. The aperture increases are modest though: about 12 μm for the 20 MPa pressure at 1 m and 2 μm at 4 m distance.

Contents

1	Introduction and background	7
1.1	General	7
1.2	General description of KBS-3H repository design	7
1.3	Scope	8
1.4	Tools	9
	1.4.1 Analytical methods	9
	1.4.2 3DEC	9
1.5	Sign convention	9
2	Olkiluoto repository	11
2.1	Site description	11
	2.1.1 Geology	11
	2.1.2 Rock data	11
2.2	Initial conditions	12
2.3	Layout	12
2.4	Heat load	12
2.5	Importance of layout assumptions	14
2.6	Time-scales	18
3	3DEC near-field models	19
3.1	Geometry	19
3.2	Finite difference zone generation	20
3.3	Material properties	20
3.4	Initial conditions	21
3.5	Thermal load	22
3.6	Boundary conditions	22
	3.6.1 Excavation phase	22
	3.6.2 Thermal phase	23
3.7	Model map	24
3.8	Calculation sequence	26
	3.8.1 Initial equilibrium	26
	3.8.2 Excavation	26
	3.8.3 Heating	26
	3.8.4 Swelling pressure and gas pressure	27
3.9	Results presentation	28
4	Results	29
4.1	Base case	29
	4.1.1 Major principal stresses and displacements at canister mid-length	29
	4.1.2 Major principal stress and displacements between canister positions	29
4.2	Relevance of boundary conditions	31
4.3	Stress field	32
	4.3.1 Stress magnitudes	32
	4.3.2 Stress orientation	32
4.4	Influence of joint and internal drift pressure	34
5	Result, summary and discussion	39
5.1	General	39
5.2	Excavation	39
	5.2.1 Stresses along the perimeter	39
	5.2.2 Spalling risk	40
	5.2.3 Reactivation (opening) risk	41

5.3	Thermal phase	43
5.3.1	Thermal disturbance – general	43
5.3.2	Perimeter stresses after 50 years – different cases	44
5.3.3	Temporal evolution at some periphery points	45
5.3.4	Spalling risk	46
5.3.5	Reactivation (opening) risk	46
6	Summary	49
6.1	General	49
6.2	Spalling	49
6.3	Fracture opening	50
6.4	Relevance and validity, future work	50
	References	51
	Appendix 1 Revision of olkiluoto KBS-3H Lay-out adaptation	53
	Appendix 2 List of Input Parameters for KBS-3H process report and evolution report	59

1 Introduction and background

1.1 General

SKB and Posiva are performing an R&D programme over the period of 2002–2007 with the overall aim to find out whether the KBS-3H concept can be regarded as an alternative to the KBS-3V concept for disposal of spent nuclear fuel. In the KBS-3H repository concept canisters with spent nuclear fuel are deposited horizontally in 300 m long deposition drifts at depth of about 400 m below the ground surface. The excavation of drifts and subsequent heat release from the canisters will produce stresses in the rock surrounding the repository. This report evaluates the stresses and displacements on the drift perimeter based on bedrock data from the Olkiluoto site in Finland for two cases:

- The drifts (or rather some drift sections) are dry, *i.e.* there is no support pressure from swelling bentonite,
- The presence of 10 MPa –30 MPa internal drift pressure (gas or swelling pressure).

The magnitude of the tangential stresses depends on:

- the heat load, *i.e.* number of canisters and the initial power and decay-rate of the spent fuel,
- the rock's thermo-mechanical properties,
- *in situ* stresses of the rock and their orientation with respect to the drifts.

Two concerns are addressed here:

- The risk of spalling in highly stressed parts of the drift periphery,
- The risk of reactivation (or rather opening) of fractures intersecting the drifts. This is in particular a concern for fractures that are approximately parallel to the drift.

Intact rock subjected to stresses amounting to 45–50% /Posiva 2007/ of the uni-axial compressive strength might damage (fail) if the confining pressure is low (spalling). Spalling is most likely to occur in the drift floor and roof areas where the largest tangential stresses are found.

A swelling high density buffer or gas produced by corrosion may exert significant pressure on the drift walls and might reactivate natural fractures in the rock. Normally drifts should be oriented and located such that they are not parallel to any main fractures. However, we present a “worst case scenario” with one fracture parallel to the drift and almost perpendicular to the smallest principal stress. This means that the initial compression on the joint is small. Internal drifts pressures with magnitudes comparable with the smallest principal stress might be enough to reactivate the joint.

1.2 General description of KBS-3H repository design

KBS-3H design is a variation of KBS-3 concept and an alternative to KBS-3V design. KBS-3H design is based on emplacement of spent fuel canisters in horizontal direction in contrary to KBS-3V design where the canisters are emplaced in vertical direction, see Figure 1-1. The repository at the Olkiluoto site is planned to be built at the depth of –420 m below sea level.

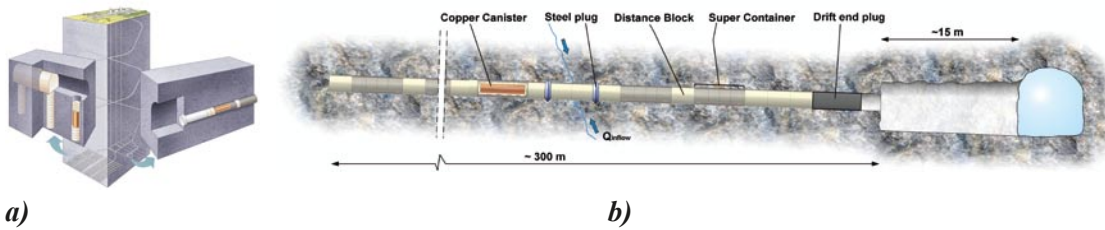


Figure 1-1. a) Principle of KBS-3V (on left) and KBS-3H (on right) repository design and b) a more detailed illustration of KBS-3H design. The canister is copper coloured.

In KBS-3H design the canister and buffer are placed in a perforated steel container, called Super Container, which is emplaced in a long horizontal drift. A distance plug of compacted bentonite is emplaced between each Super Container to obtain proper mutual thermal spacing and isolation.

One of the most important functions of the distance block is to seal the drift section between the Super Containers in order to prevent flow and advective transport along the drift. The sealing and plugging is assumed to occur when the distance block absorbs water (saturates), swells and obtains proper swelling pressure. KBS-3H candidate designs are at the moment being developed to proper level of details based on Olkiluoto bedrock data in order to evaluate the feasibility of the KBS-3H concept in 2007.

This study is based on using Olkiluoto specific design, where the spacing between deposition drifts is 25 m and spacing between canister midpoints is 10.9 m. Corresponding studies for the two SKB sites Forsmark and Laxemar are intended to follow. The key parameters for determination of the canister spacing and the tunnel spacing are the rock thermal conductivity and the initial undisturbed geothermal temperature. The Forsmark heat conductivity is significantly higher than the one in Olkiluoto, while the initial temperature is higher in Laxemar. This means that the detailed design for both SKB sites needs to be established before any in-depth stability analyses can be initiated.

1.3 Scope

The main issue is to determine the stresses on the drift perimeter. The results will show:

- what effects different repository layouts, *i.e.* different deposition panel geometries will have on average thermal stresses on the repository scale,
- whether spalling threshold is exceeded,
 - when,
 - by how much,
 - amount of rock volume in potential failure mode,
- near-field rock stresses and displacements at the periphery of different drift segments (at canister mid-length and between canister positions),
- effects of different *in situ* stress magnitudes and orientations,
- effects of 10 MPa –30 MPa internal drift pressures.

1.4 Tools

1.4.1 Analytical methods

Thermal analytical solution

The thermal analytical solution derived by /Claesson and Probert 1996a/ is based on a rectangular (panel) far-field solution. It has been implemented for near-field temperature analyses by /Hökmark and Fälth 2003/. This is done whereby the panel solution in a “window” is subtracted and replaced by 33 individual canisters. The canister studied and its two nearest neighbours are represented by compound line sources /Hökmark and Fälth 2003/, the second nearest neighbours by ordinary line sources and the remaining canisters in the window are represented by point sources. The line source solution is identical to the one given by /Ikonen 2003/. A schematic overview of the process is given in Figure 1-2.

Thermo-mechanical analytical solution

The thermo-mechanical analytical solution derived by /Claesson and Probert 1996b/ gives a good representation of the average repository-scale stresses and displacements, and can therefore be used with good accuracy to generate thermo-mechanical boundary conditions /Probert and Claesson 1997/. This solution, however, does not take into account cavities in the rock or the actual distribution of the heat sources and cannot be used to determine near-field stresses and displacements around an individual canister.

The analytical solution is used here to determine how different repository layouts affect stresses and to derive thermo-mechanical boundary conditions for the numerical 3DEC models.

The two analytical solutions have been implemented for use in a commercial mathematical spreadsheet program (MathCad).

1.4.2 3DEC

3DEC is a numerical **3**-dimensional **D**istinct **E**lement **C**ode /Itasca 2003/. In the model the discontinuous medium, *i.e.* rock mass, is represented by deformable blocks, which are divided into a mesh of finite difference elements (see Section 0 for zone sizes in the near-field models).

Temperatures and temperature increments at each gridpoint in the model are calculated using a built-in analytical solution based on regular grids of point sources. Here the central canisters were represented by arrays of point sources to reproduce the effects of line and compound sources as in the analytical solution (cf Figure 1-2).

Thermally induced stresses are subsequently calculated from the temperature increments above.

1.5 Sign convention

In the following analyses negative stresses are compressive.

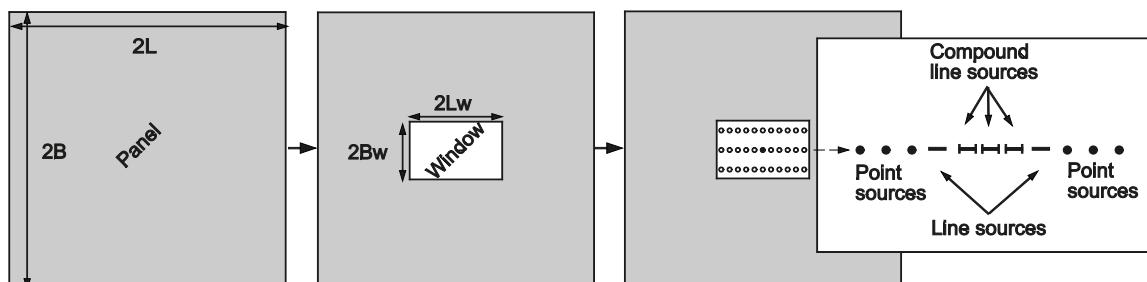


Figure 1-2. Schematic view of thermal panel solution with window.

2 Olkiluoto repository

2.1 Site description

2.1.1 Geology

The rocks at Olkiluoto (Figure 2-1) can be divided into two major groups: 1) high-grade metamorphic rocks, including various migmatitic gneisses, homogeneous tonalitic-granodioritic-granitic gneisses, mica gneisses and quartzitic gneisses, and mafic gneisses, 2) igneous rocks, including pegmatitic granites and diabase dykes. The migmatitic gneisses can further be divided into three subgroups in terms of the type of migmatite structure: veined gneisses, stromatic gneisses and diatexitic gneisses, which represent distinct end members in a gradational system of homogenous gneisses and migmatitic gneisses. The change from homogeneous gneisses to migmatitic gneiss variants and between the different types of migmatitic gneiss takes place gradually, so that it is not possible to define any natural borders between the end members. Thus, an artificial border between the homogeneous gneisses and migmatitic gneisses has been set at a 10% proportion of the leucosome. The veined gneisses account for 43% of the volume of the Olkiluoto study area, the stromatic gneisses for 0.4% and the diatexitic gneisses for 21%. The granite pegmatites make up 20% of the bedrock, the tonalitic-granodioritic-granitic gneisses 8%, mica gneisses 7% and the mafic gneisses 1%, based on the lithological description of numerous cored boreholes /Paananen et al. 2006/.

2.1.2 Rock data

Values of material property parameters (Table 2-1) were derived from Posiva site reports /Posiva 2005, 2007/.

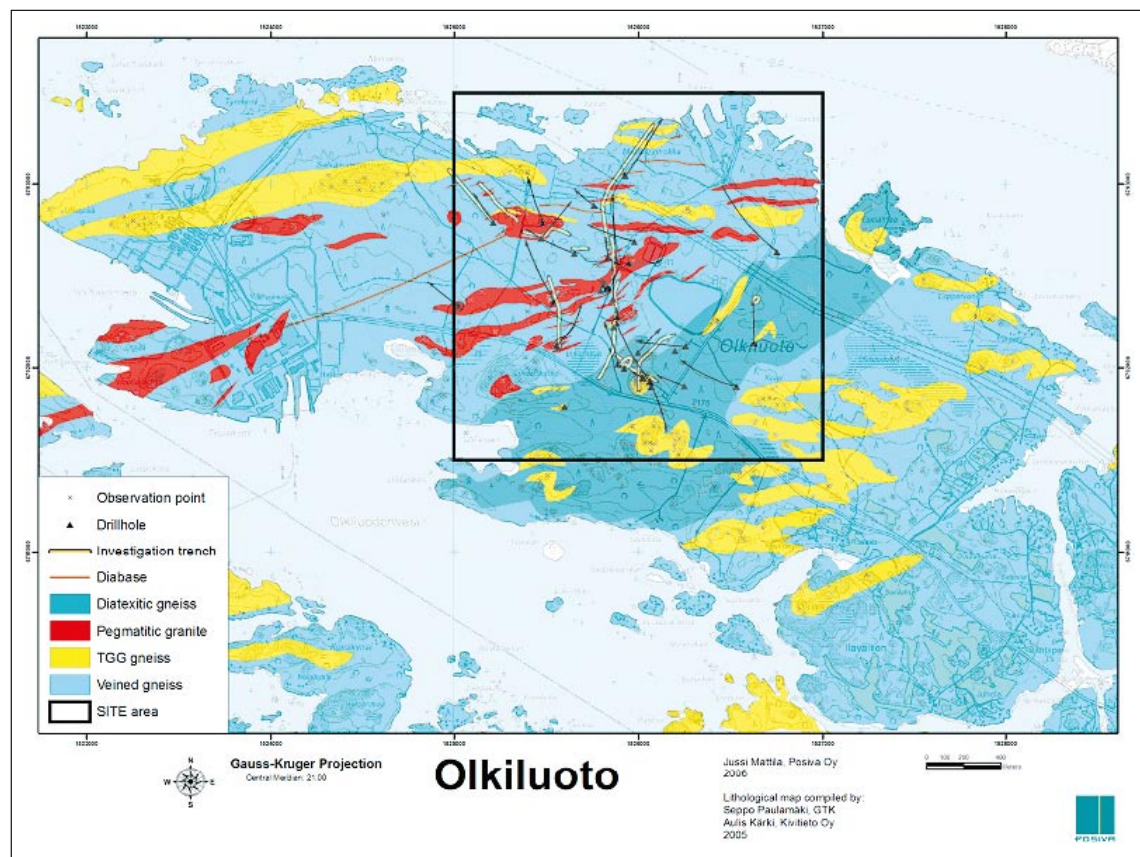


Figure 2-1. Rock types at the Olkiluoto site /Paulamäki et al. 2006/.

Table 2-1. Material properties.

	Rock mass	Intact rock
Density (ρ)	2,754 kg/m ³	2,754 kg/m ³
Heat conductivity (λ)	2.7 W/(m K)	2.7 W/(m K)
Heat diffusivity (a)	1.23·10 ⁻⁶ m ² /s	1.23·10 ⁻⁶ m ² /s
Linear expansion coefficient (α)	9.5·10 ⁻⁶ K ⁻¹	9.5·10 ⁻⁶ K ⁻¹
Young's modulus (E)	50 GPa*	60 GPa
Poisson's ratio (ν)	0.25	0.25

* Rock mass modulus of 50 GPa means normal, moderate jointing regime i.e. joint spacing 2 m and normal joint stiffness 150 GPa/m as indicated in Table 3-2.

2.2 Initial conditions

The major principal stress, σ_1 , is sub-horizontally oriented (dipping 20°) and is oriented about 90–120° with respect to North /Posiva 2005, 2007/. The intermediate and minor principal stresses vary significantly in orientation. There are considerable uncertainties regarding magnitudes. The ranges are shown in Table 2-2.

In the following it will be assumed that σ_h is a principal stress.

The initial *in situ* temperature of the rock mass is set to 10.5°C at 400 m (see Appendix 2). This figure does not have influence on the stress-strain analyses performed here.

2.3 Layout

Figure 2-2 shows the repository-scale layout and the stress orientation schematically. Drifts are perpendicular to σ_h , i.e. σ_1 is sub-parallel to the drifts. It is also assumed that σ_h is the minor horizontal principal *in situ* stress. Figure 2-3 shows layout data for canisters and drifts.

2.4 Heat load

All canisters are assumed to have an initial power of 1,700 W. The power decay is assumed to be that of SKB reference fuel /Hökmark and Fälth 2003/, cf Figure 2-4.

Table 2-2. Stress magnitudes at 400 m depth.

Stress (at 400 m)	σ_H	σ_V	σ_h
Lower limit	13.4 MPa	6 MPa	8.4 MPa
Upper limit	26.8 MPa	12 MPa	15.8 MPa

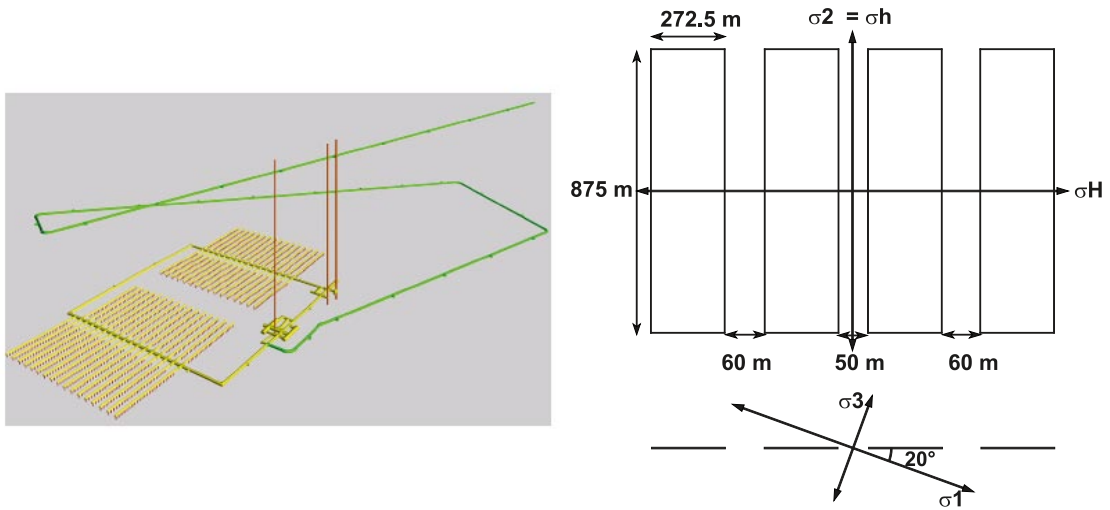


Figure 2-2. Schematic overview of generic (base case) repository /Ikonen 2003/ (left). In situ stress orientation with respect to panels: horizontal cross section (top right) and vertical cross section (bottom right). Drifts are oriented across panels (along σ_H).

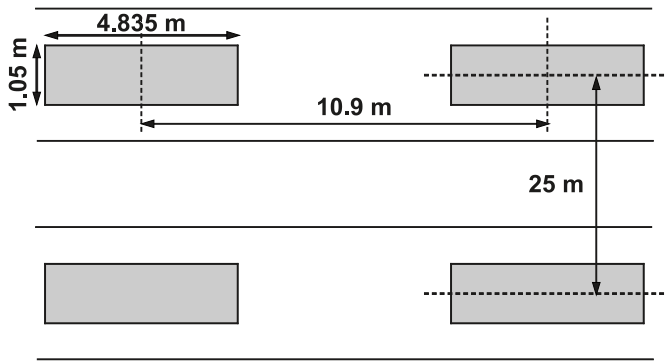
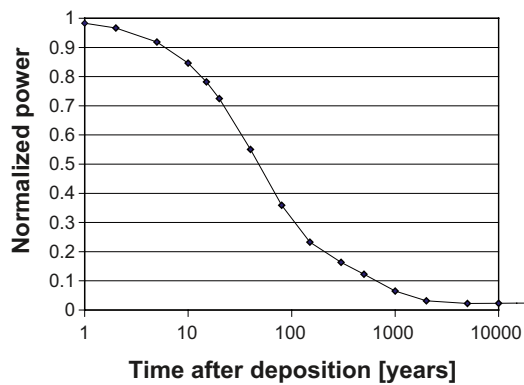


Figure 2-3. Layout data see Appendix 2. Note: Not to scale.



The power function is given by the following expression:

$$P(t) = P(0) \sum_{i=1}^7 a_i \exp(-t/t_i),$$

where $P(0) = 1,700$ W

(see Table 2-3 for exponential coefficients)

Figure 2-4. Normalized power function.

Table 2-3. Decay-coefficients for SKB reference fuel /Hökmark and Fäth 2003/.

i	t [years]	a_i [-]
1	20	0.0601473
2	50	0.705024
3	200	-0.054753
4	500	0.2497671
5	2000	0.0254075
6	5000	-0.009227
7	20,000	0.0238767

2.5 Importance of layout assumptions

In order to get a picture of how different repository layouts influence thermally induced stresses and displacements the thermo-mechanical analytical solution /Claesson and Probert 1996b/ is applied to a site-adapted KBS-3H layout (6 panels) presented in Appendix 1 and to the generic rectangular repository with 4 panels (cf Figure 2-2) The generic layout solution is similar to the one analyzed by /Ikonen 2003/. The two layout solutions have practically identical total heat loads. The site-adapted 6-panel-repository has 3,432 canister locations and the 4-panel-repository has 3,500 canister locations. The actual amount of canisters is 3,000 but to cover the uncertainties (unusable rock) the layout must be adapted to accommodate an excess number of canister locations.

Stresses are calculated at repository level at the centre of panel 1 (horizontal position marked with a dot in Figure 2-5 and Figure 2-6). These are compared in Figure 2-7 (left). Displacements (shown in Figure 2-7 (right)), with respect to drift centre (marked with a dot), are calculated at ± 40 m (along drift), ± 12.5 m (across drift) and ± 40 m (vertically). These distances correspond to the boundaries of the near-field models in Section 3.

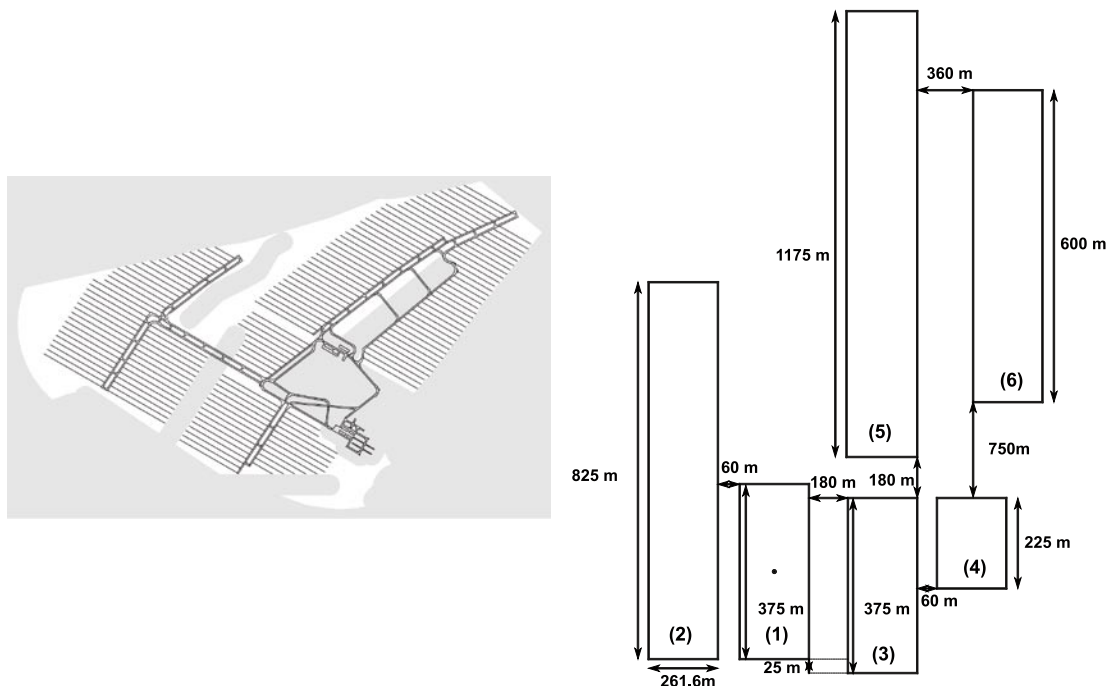


Figure 2-5. KBS-3H layout at Olkiluoto site (Appendix 1, left) and schematic layout (right). The dot marks the point that is analyzed.

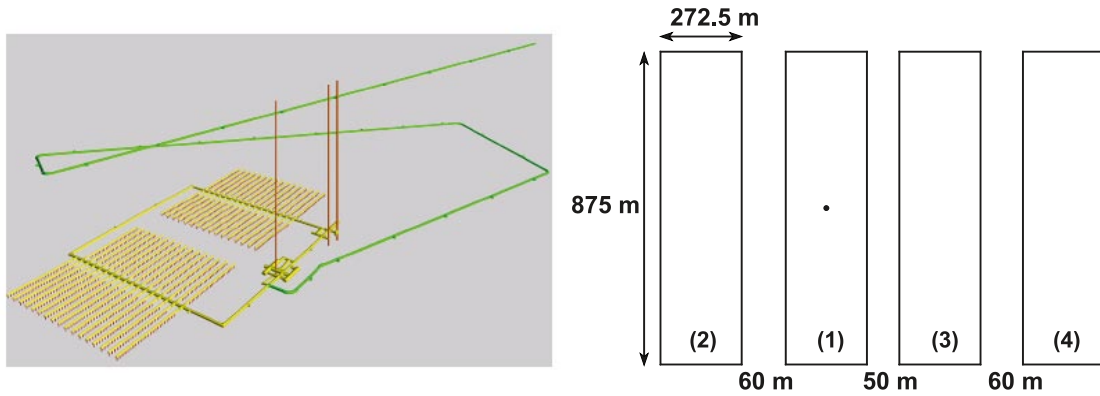


Figure 2-6. Generic repository layout /Ikonen 2003/, left, and schematic layout, right. The dot marks the point that is analyzed.

Figure 2-8 shows the rock wall temperature for canister positions corresponding to the dots in the two layouts.

Figure 2-9, Figure 2-10 and Figure 2-11 show average repository scale stresses across drifts, along drifts and vertically for a number of positions within the two layouts.

As seen in Figure 2-7 and Figure 2-8, differences in horizontal stress additions between the 6 panel site-adapted layout and the 4 panel generic layout are small (about 1.5 MPa at most during the first 100 years after deposition). The difference in vertical stress additions is a bit larger, but still less than about 3 MPa. This means that the regular generic layout gives a sufficiently good representation of the processes within the rock mass for the time-scales used in this investigation (0–500 years) and can be used to obtain mechanical boundary conditions for near-field models that are also relevant to the detailed site adapted layout.

Note that the comparison made above relates to the specific points indicated in Figure 2-5 and Figure 2-6. There are also differences between positions in different panels. Figure 2-9, Figure 2-10 and Figure 2-11 show stresses in the centre of a number of panels. The horizontal stress across drifts in panel 5 is 1 MPa larger than the corresponding stress in the generic 4 panel layout. All horizontal stresses along the drifts are less than the corresponding stress in the generic layout. The largest horizontal stress along drifts is found in panel 4 (0.2 MPa less than in the generic layout). The smallest stress is found in panel 5 (2.3 MPa less).

The differences are small enough that the point selected for analysis here (centre of panel 1 in the generic layout) can be regarded as representative of the Olkiluoto KBS-3H repository as a whole, at least for the central parts of each panel.

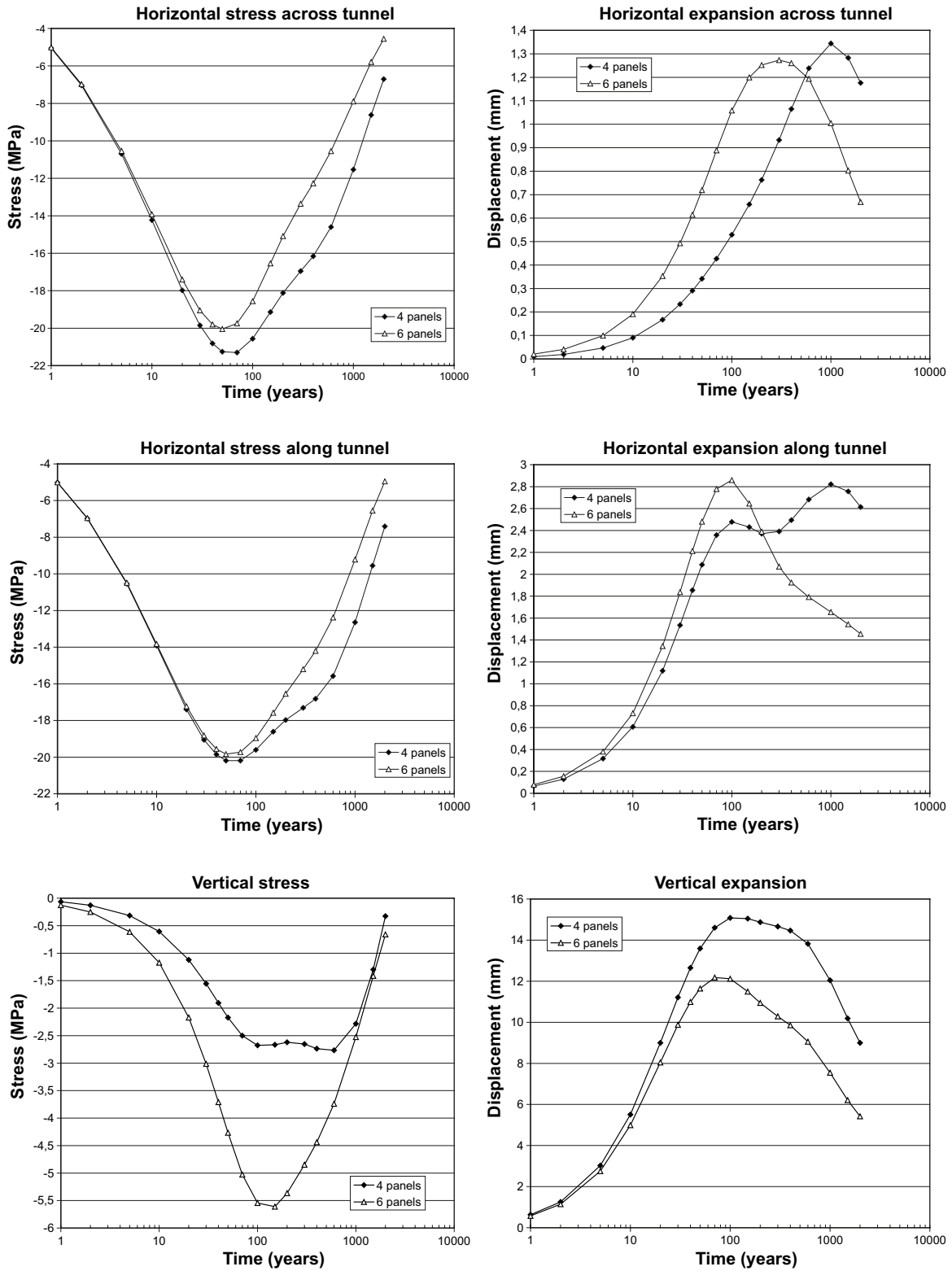


Figure 2-7. Stress and displacement comparison. Displacements regard points at 12.5 m horizontal (upper), 40 m horizontal (centre) and 40 m vertical (bottom) distance from the selected points.

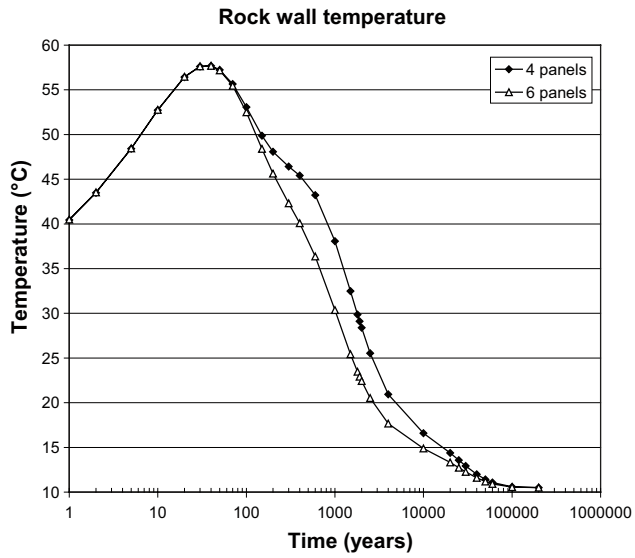


Figure 2-8. Rock wall temperature comparison.

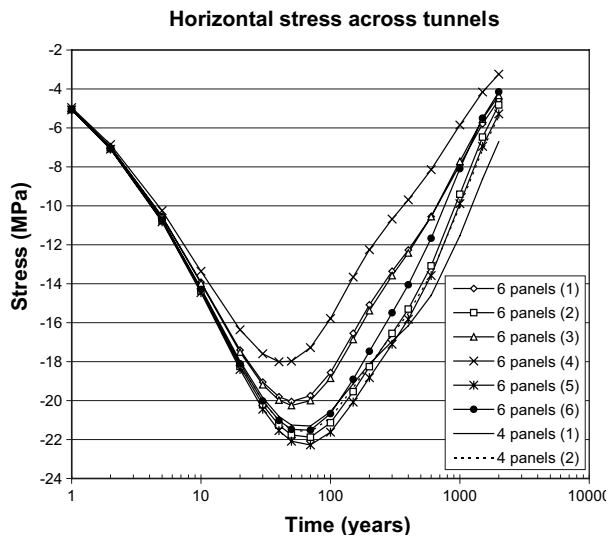


Figure 2-9. Horizontal thermal stresses across drifts at given panel centres (numbered as in Figure 2-5 and Figure 2-6).

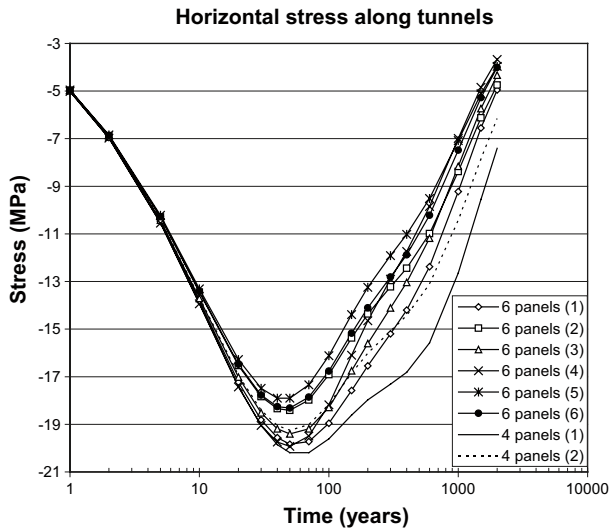


Figure 2-10. Horizontal thermal stresses along drifts at given panel centres (numbered as in Figure 2-5 and Figure 2-6).

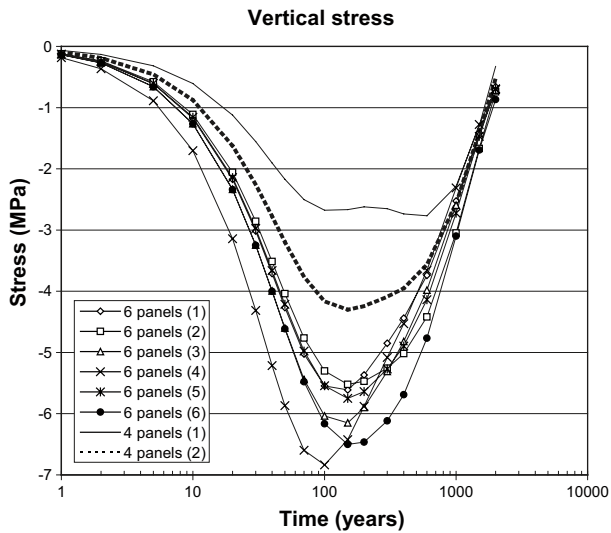


Figure 2-11. Vertical thermal stresses at given panel centres (numbered as in Figure 2-5 and Figure 2-6).

2.6 Time-scales

The stresses on the drift perimeter reach their maxima after 50 to 75 years (see Section 4). This is somewhat earlier than the average repository scale stress maxima in the above figures. It is also worth noting that the stress maxima occur some 20 to 30 years after the rock wall temperature has reached its maximum (30–40 years, see Figure 2-8).

3 3DEC near-field models

3.1 Geometry

Olkiluoto repository for spent nuclear fuel is located 400 m below the ground surface. The near-field models relate to a portion of rock around the point indicated in Figure 2-6. Figure 3-1, below, shows a cut-through view of a near-field model, *i.e.* it is symmetric with respect to the drift axis. The central part of the model, *i.e.* the width, length and 12.5 m above and below the drift, is modelled with “intact rock” properties (see Table 3-1). There is one “fictitious¹” joint parallel to the drift and running through the centre of the model at $y = 0$ (see Figure 3-6, left, and Table 3-2 for joint properties).

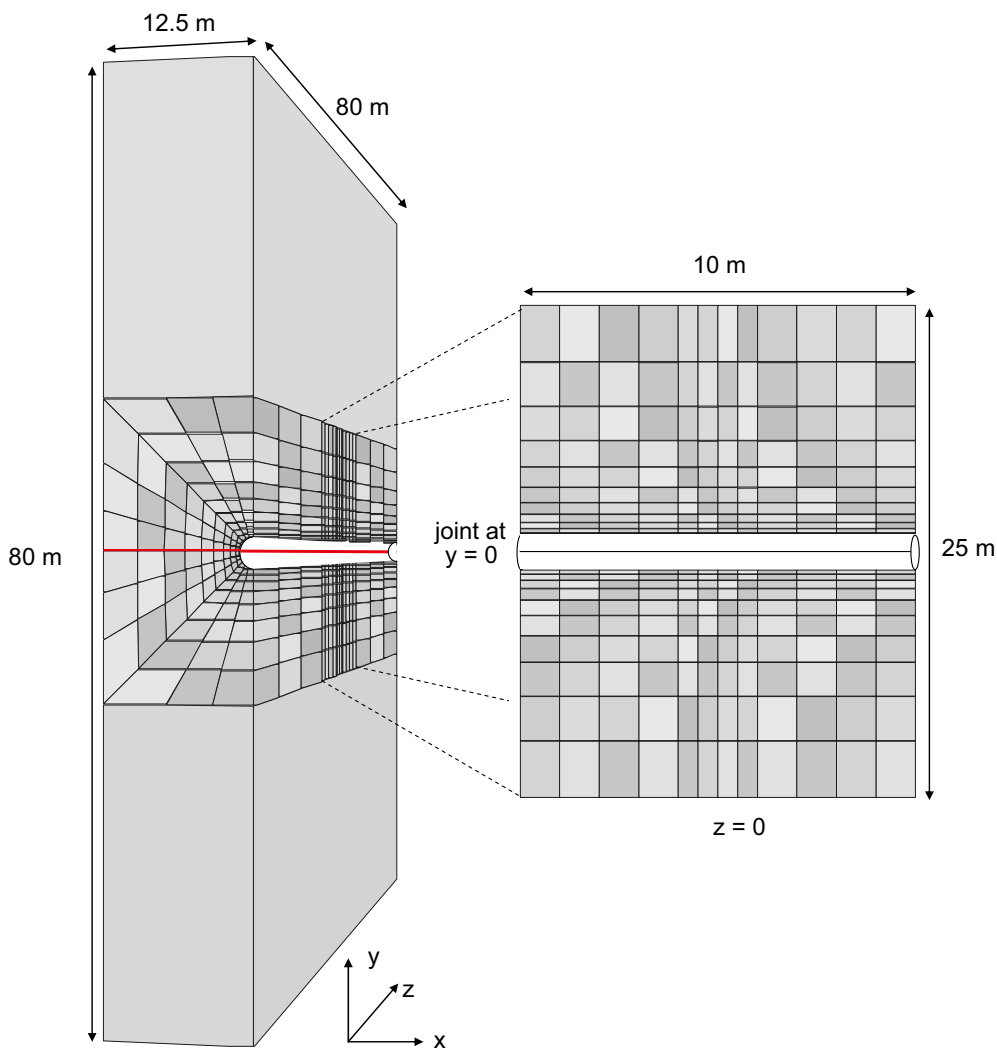


Figure 3-1. 3DEC model geometry.

¹ This joint will be made active for the model with internal drift pressure (cf Table 3-5).

Table 3-1. Material properties.

	Rock mass	Intact rock
Density (ρ)	2,754 kg/m ³	–
Heat conductivity (λ)	2.7 W/(m K)	–
Diffusivity (α)	1.23·10 ⁻⁶ m ² /s	–
Volume expansion (α)	9.5·10 ⁻⁶ K ⁻¹	–
Young's modulus (E)	50 GPa*	60 GPa
Poisson's ratio (ν)	0.25	0.25

* Rock mass modulus of 50 GPa means normal, moderate jointing regime i.e. joint spacing 2 m and normal joint stiffness 150 GPa/m as indicated in Table 3-2.

Table 3-2. Joint properties.

	Fictitious joints	Active joints
Cohesion	500 MPa	0.5 MPa
Normal stiffness	20,000 GPa/m	150 GPa/m
Shear stiffness	20,000 GPa/m	40 GPa/m
Tensile strength	500 MPa	0 MPa
Friction	45°	34°

3.2 Finite difference zone generation

The central 4 m along the drift in a hollow cylinder of outer radius 1.2 m (drift interior has zone length 0.5 m) has zone edge length 0.08 m. The outer cylindrical shell (of the same length and outer radius 1.6 m) has zone edge length 0.22 m. The edge length increases with distance from the central part to 5 m at the boundaries.

3.3 Material properties

Material properties given in Table 3-1 are derived from Posiva site reports /Posiva 2005, 2007/.

Joint properties for both active and fictitious joints are given in Table 3-2. These properties are the same as in SKB's preliminary site descriptions for the Forsmark and Laxemar sites /SKB 2005, 2006a/.

In reality joints will have varying, uncertain and stress-dependent properties. In particular the stiffness values will depend on the fracture normal stress. The normal stiffness value selected here is, however, reasonably representative of fractures in low compression, such as the horizontal fracture that intersects the pressurized tunnel in the present model. Figure 3-2 shows the selected stiffness compared with typical stress-stiffness relations considered in SKB's near-field analyses /Hökmark et al. 2006/. Given the symmetry assumed here and the consequently small shear load, details of the shear properties (friction, cohesion, joint shear stiffness) have little importance.

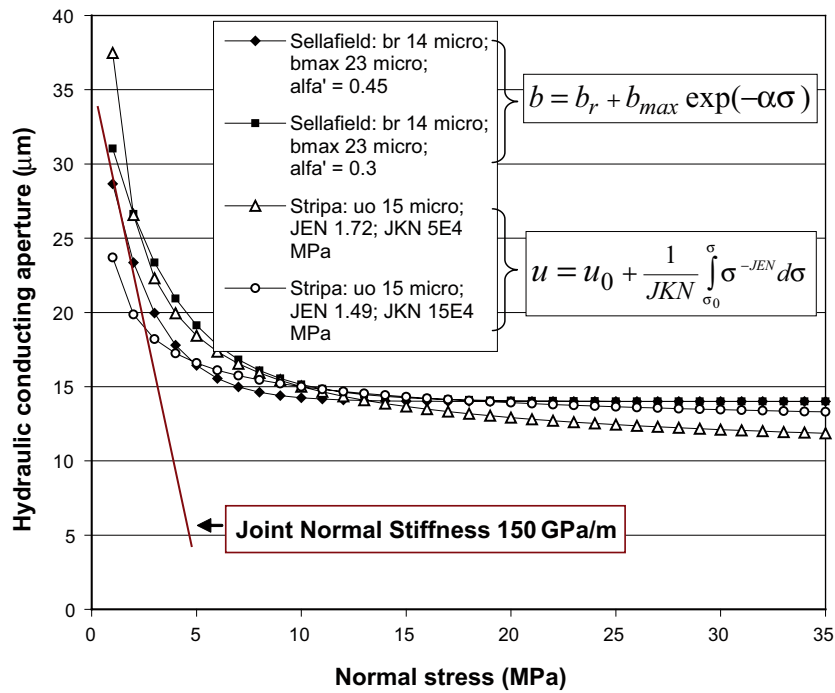


Figure 3-2. Joint normal stiffness value compared with typical stress-aperture relations /Hökmark et al. 2006/.

3.4 Initial conditions

Stress orientations for four near-field models are presented in Table 3-3. As seen in Figure 3-1 the model axes are oriented such that σ_{xx} is across drifts, σ_{yy} is vertical and σ_{zz} is along drifts. Figure 3-3 shows the *in situ* stress orientations schematically.

The major principal stress, σ_1 , is either sub-horizontally oriented (20°) and parallel to the drift with σ_{yz} the only non-zero shear stress (models A and E) or perfectly parallel/perpendicular to the drift (models F and G). Note that (G) is a hypothetical case which is considered here just to complete the picture. In reality the deposition drifts will always be approximately parallel with the major stress.

The initial *in situ* temperature of the rock mass is 10.5°C at 400 m.

Table 3-3. Stress magnitudes at 400 m depth.

Stress (at 400 m)	σ_{xx}	σ_{yy}	σ_{zz}	σ_{yz}
Upper limit (A, base case)	15.8 MPa	12 MPa	26.8 MPa	6.2 MPa
Lower limit (E)	8.4 MPa	6 MPa	13.4 MPa	3.1 MPa
Perfect symmetry I (F)	15.8 MPa	9.7 MPa	29.1 MPa	0 MPa
Perfect symmetry II (G)	29.1 MPa	9.7 MPa	15.8 MPa	0 MPa

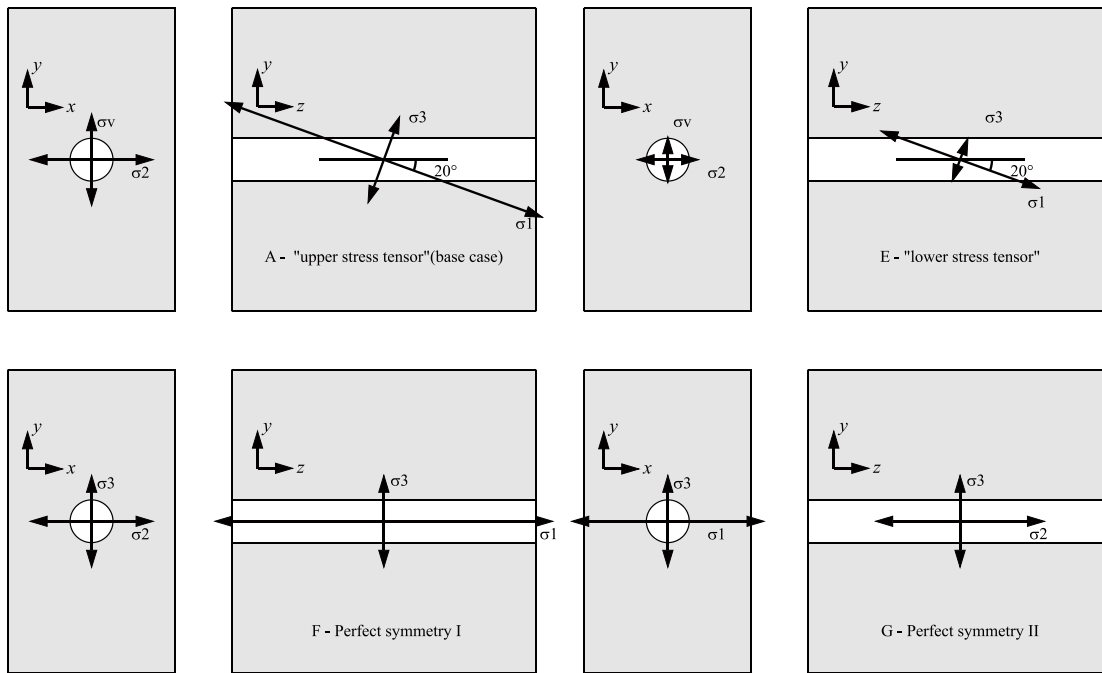


Figure 3-3. Stress orientations with respect to the near-field model.

3.5 Thermal load

As seen in Section 2.5 the differences in stresses and rock wall temperature between the layouts in Figure 2-5 and Figure 2-6 are sufficiently small that the generic layout (Figure 2-6, right) can be used (*i.e.* to specify heat source distribution and mechanical boundary conditions) in the following analyses. The thermal load is presented in Table 3-4.

3.6 Boundary conditions

3.6.1 Excavation phase

Roller boundaries are used on all boundaries (see Figure 3-4, top), *i.e.* the assumption is that the vertical planes in the yz -cross section are symmetry planes even though that is not strictly the case because of the dipping major stress.

Table 3-4. Thermal load.

Canister spacing	10.9 m
Canisters per drift	25
Drift spacing	25 m
Drifts per panel	35
Initial power per canister	1,700 W
Power decay	Cf Table 2-3

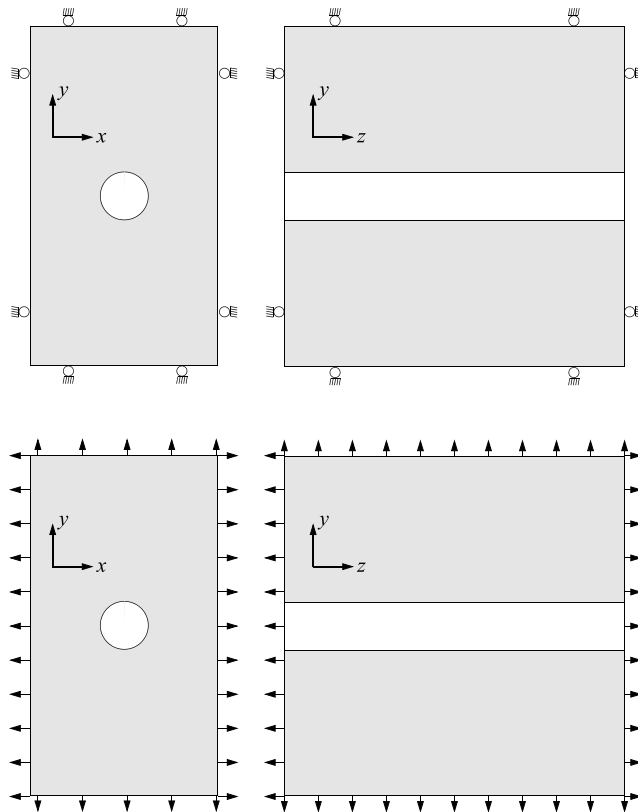


Figure 3-4. Boundary conditions: roller boundaries for excavation (top) and expansion/contraction relative to the drift centre (bottom) for the thermal phase (not to scale).

3.6.2 Thermal phase

For the thermal phase three sets of boundary conditions are selected:

1. Roller boundaries on all vertical sides, *i.e.* there are no horizontal movements, but the top and bottom of the model are allowed to expand and contract according to Figure 3-5. This is referred to as model B (cf section 4.2).
2. Relative normal movements of the boundaries with respect to the drift centre (base case, model A, cf Figure 3-4).
3. Same as above with the exception that there is a vertical stress boundary on top of the model (Model I, cf section 0). Note that this works well only for models with principal *in situ* stresses oriented along model axes.

All time-dependent boundary conditions (displacements as well as stresses) are derived using the analytical thermo-mechanical solution /Claesson and Probert 1996b/ (cf Figure 2-7). The second case (with upper limit stress tensor in Table 3-3) is used for reference in further analyses.

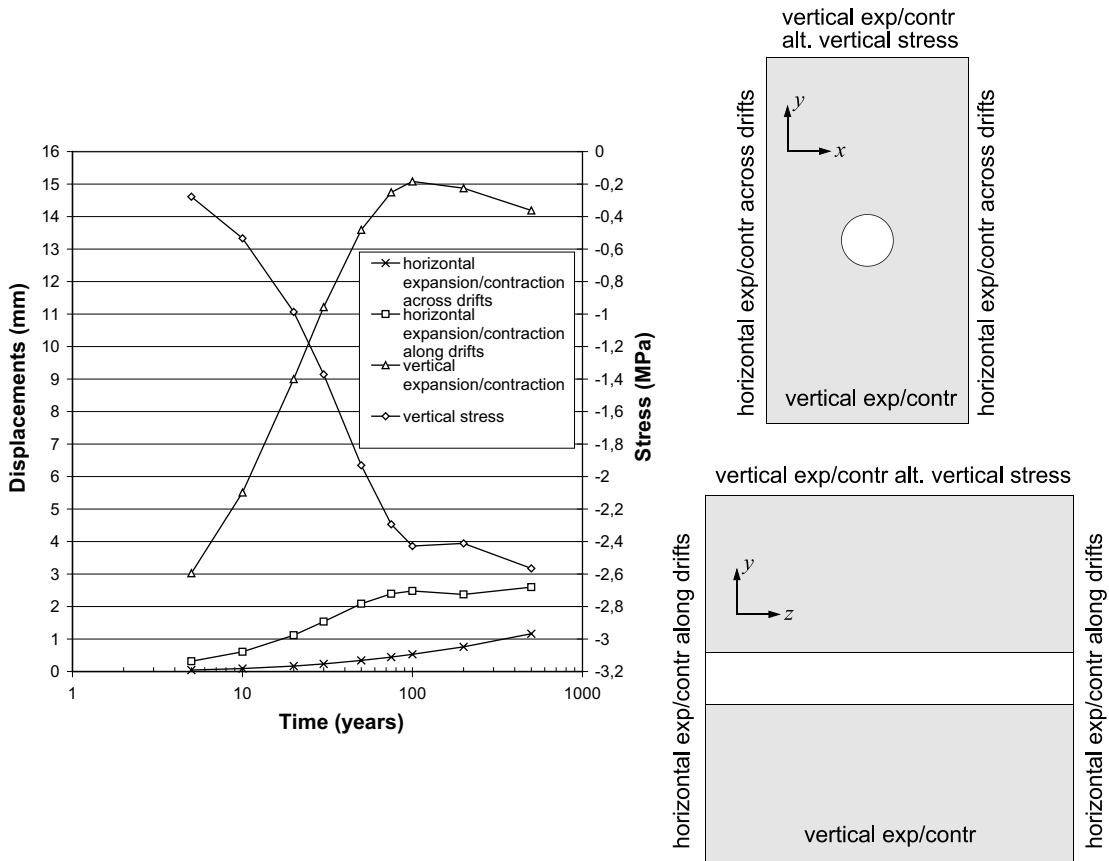


Figure 3-5. Boundary conditions for 3DEC near-field models. Vertical stress boundary only for model I (in situ stresses oriented along model axes).

3.7 Model map

Model A (Table 3-5) is taken to be the reference case with which all subsequent models are compared.

As the movements of the vertical boundaries are small (Figure 3-5), a model with fixed vertical boundaries (B), is run to confirm that preventing the vertical boundaries to move in their normal directions (*i.e.* ignoring the expansion of the modeled rock volume) will overestimate the stresses on the drift perimeter.

Model C has the same initial and boundary conditions as Model A, but with one active horizontal joint (cf Figure 3-6). There are three different sub-cases:

- No swelling pressure,
- Internal drift pressures between 10 to 30 MPa are applied in the backfilled drift immediately after excavation (this is equivalent to a state after some thousand years when the thermal pulse has passed and the stresses have settled to their post-excavation magnitudes),
- Internal drift pressures between 10 to 30 MPa are applied in the backfilled drift after 100 years.

Models A and D are identical with the only difference that stresses are determined at canister mid-length in model A and between two canister positions in model D. The results from the two models will give an estimate of how the risk of spalling and possible opening of the joint varies along the drift.

Table 3-5. Olkiluoto model map.

Model code	<i>In-situ</i> stress	Thermal phase	
A	$\sigma_1 = 29.1$ MPa $\sigma_2 = 15.8$ MPa $\sigma_3 = 9.7$ MPa dip $\sigma_1 = 20^\circ$	Expanding boundaries	max stress tensor (see Table 3-3) “base case”
B	$\sigma_1 = 29.1$ MPa $\sigma_2 = 15.8$ MPa $\sigma_3 = 9.7$ MPa dip $\sigma_1 = 20^\circ$	Roller boundaries on vertical boundaries Expanding horizontal boundaries	
C	$\sigma_1 = 29.1$ MPa $\sigma_2 = 15.8$ MPa $\sigma_3 = 9.7$ MPa dip $\sigma_1 = 20^\circ$	Expanding boundaries	One active joint and swelling pressures of 10 to 30 MPa either applied in backfilled drift or after 100 yr heating
D	$\sigma_1 = 29.1$ MPa $\sigma_2 = 15.8$ MPa $\sigma_3 = 9.7$ MPa dip $\sigma_1 = 20^\circ$	Expanding boundaries	Tangential stresses and displacements between canister positions of the base case
E	$\sigma_1 = 14.5$ MPa $\sigma_2 = 8.4$ MPa $\sigma_3 = 4.9$ MPa dip $\sigma_1 = 20^\circ$	Expanding boundaries	min stress tensor (see Table 3-3)
F	$\sigma_1 = 29.1$ MPa $\sigma_2 = 15.8$ MPa $\sigma_3 = 9.7$ MPa dip $\sigma_1 = 0^\circ$	Expanding boundaries	Perfect symmetry σ_1 along drift
G	$\sigma_1 = 29.1$ MPa $\sigma_2 = 15.8$ MPa $\sigma_3 = 9.7$ MPa dip $\sigma_1 = 0^\circ$ dd $\sigma_1 = 90^\circ$	Expanding boundaries	Perfect symmetry σ_2 along drift
H	$\sigma_1 = 0$ MPa $\sigma_2 = 0$ MPa $\sigma_3 = 0$ MPa	Expanding boundaries	No <i>in situ</i> stresses
I	$\sigma_1 = 29.1$ MPa $\sigma_2 = 15.8$ MPa $\sigma_3 = 9.7$ MPa dip $\sigma_1 = 0^\circ$	Expanding boundaries; vertical stress boundary on top of model	Perfect symmetry σ_1 along drift

Models A, E, F, and G have the same thermal load and boundary conditions but different *in situ* stress magnitudes and orientations. The results from these models are compared in order to determine the effect on tangential stresses of variations in initial conditions. Model G is an event unlikely to occur as it can be avoided by aligning the drifts with the major principal stress.

Model H has the same thermal load and boundary conditions as models A, E, F, and G but with all *in situ* stresses set to zero.

Model I verifies that, for *in situ* stresses oriented along model axes, having a vertical stress boundary on top of the model can be used interchangeably with an expanding/contracting top boundary.

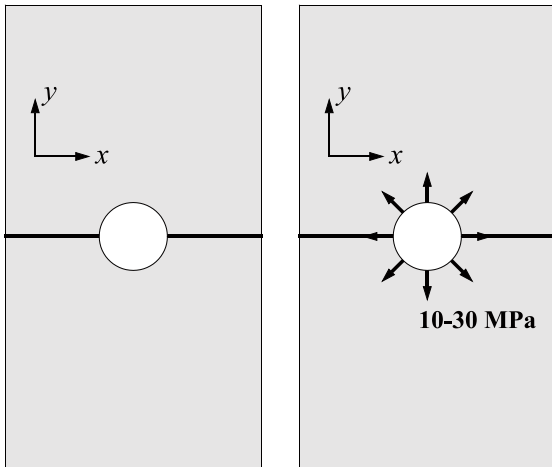


Figure 3-6. Model C with horizontal joint and no swelling pressure (left) and swelling pressures between 10 and 30 MPa (right).

3.8 Calculation sequence

The numerical calculation is done in three major steps:

- Initial equilibrium,
- Excavation of deposition drift,
- Heating.

3.8.1 Initial equilibrium

The initial conditions (*i.e.* *in situ* stresses) are set according to Table 3-5 and the model is taken to equilibrium. Note that models with *in situ* principal stress aligned with the co-ordinate axes (F, G, I) are in equilibrium from the start.

3.8.2 Excavation

The deposition drift is excavated in 12 steps as seen in Figure 3-7. This is done in order to determine displacements on the drift perimeter as the drift front approaches and passes the centre of the model section.

3.8.3 Heating

The thermal load and decay rate are given by Figure 2-3 and Table 2-3. Far away canisters give little individual contribution and are combined in groups of five for increased calculation speed. As seen in Figure 3-8 this approximation gives identical results compared with modelling every canister individually.

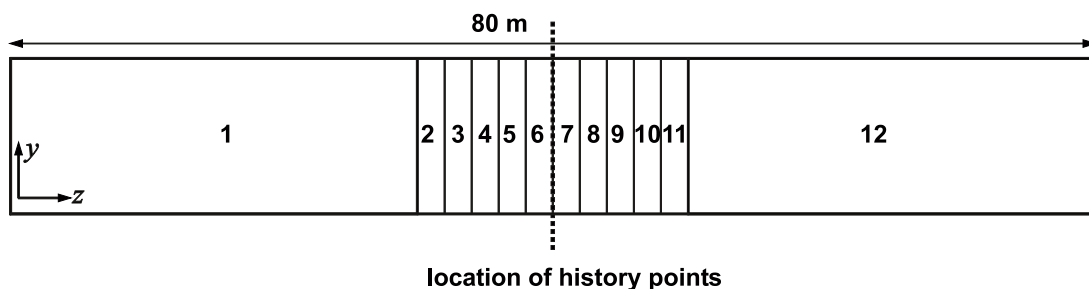


Figure 3-7. Schematic drawing of step-wise excavation. Excavation steps 2 –11 are 2 m in length. The dotted line marks location of 3DEC history points at the centre of the drift.

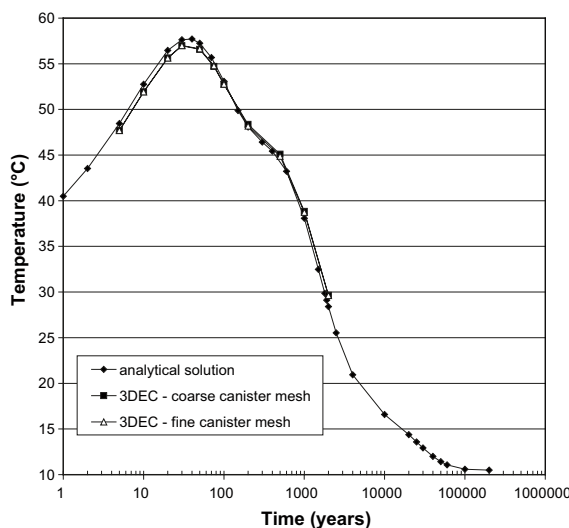


Figure 3-8. Rock wall temperature comparison between the analytical solution and 3DEC.

3.8.4 Swelling pressure and gas pressure

For the model with an active joint (C) three different cases are looked at:

- The drifts remain dry and there is no internal pressure.
- The drifts are backfilled (using the “fill” command in 3DEC) directly after excavation and internal drift pressures of 10, 15, 20, 25 and 30 MPa are applied.
- The drifts are backfilled after 100 years and internal drift pressures of 10, 15, 20, 25 and 30 MPa are applied.

Buffer material properties are given in Table 3-6. Note that the properties of the buffer material are unimportant to the calculations since the stresses within the drift are specified explicitly.

Relevant mechanical models of saturated or unsaturated buffer materials are significantly more complicated than the simple elastic model used here. The conceptual buffer model and the actual parameter values are however unimportant in this case.

Table 3-6. Buffer material properties.

	Buffer material
Density (ρ)	2,000 kg/m ³ *
Linear thermal expansion (α)	9.5·10 ⁻⁶ K ⁻¹ **
Young's modulus (E)	400 MPa***
Poisson's ratio (ν)	0.25**

* See Appendix 2

** Same values as for the rock (see Table 3-1)

*** Average value for unsaturated bentonite blocks /Kalbantner and Johannesson 2000/.

3.9 Results presentation

A number of points on (for displacements) and between 13 and 14 mm from (for stresses) the drift perimeter are specified to monitor stresses and displacements. The results are presented in diagrams showing the time evolution of the major principal stress at points 3, 10, 19, 32, and 39 on the drift perimeter (cf Figure 3-9).

A large number of additional points on the drift perimeter are also selected at specific points in time: after excavation, 50 years of heating (time of maximum tangential stress at floor and roof) and 100 years of heating (time of minimum normal stress on the joint). Here, the stress distribution along the drift perimeter is shown.

Radial displacements are presented at 45-degree-intervals (measured from the drift roof) for the excavation phase. Contour plots showing normal displacements on the joint for different internal drift pressures are presented in Section 0.

Due to the symmetry of the *in situ* stresses it is sufficient to show results from one side of the drift.

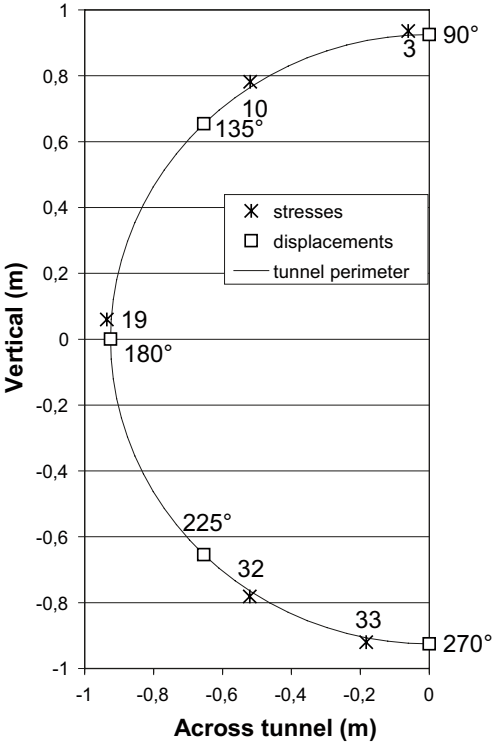


Figure 3-9. Location of history points.

4 Results

4.1 Base case

4.1.1 Major principal stresses and displacements at canister mid-length

The largest principal stress is 110 MPa (maximum value after 50 years) during the thermal phase (Figure 4-1).

As seen in Figure 4-2 and Figure 4-3 the drift has converged almost to its final post-excavation state when the drift front has advanced 4 m from the position studied. Note that negative displacements represent inward movements.

4.1.2 Major principal stress and displacements between canister positions

The stresses on the drift perimeter between canister positions are compared with those of the base case, *i.e.* at canister mid-length (Figure 4-4). The difference in stress magnitudes of the two cases is about 16 MPa after 5 years (Figure 4-5). This difference decreases steadily and is practically negligible after 500 years. The largest principal stress is of the order 102 MPa after 50 years. There are very small differences in thermally induced displacements.

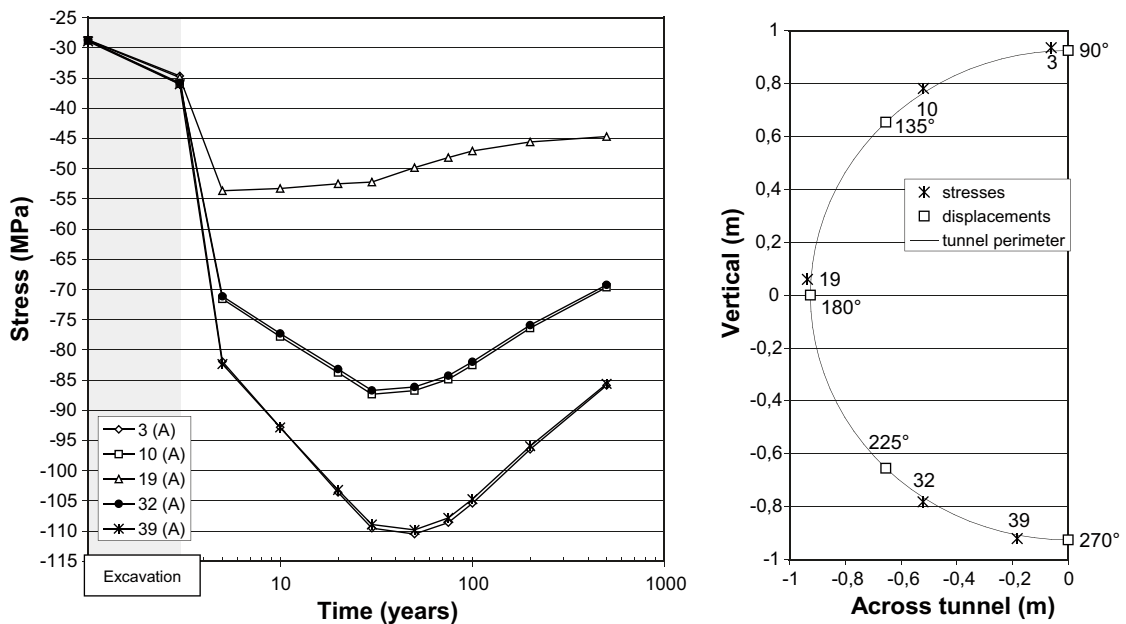


Figure 4-1. Major principal stresses during the heating phase. Grey shaded area represents non-thermal phase (primary equilibrium and excavation).

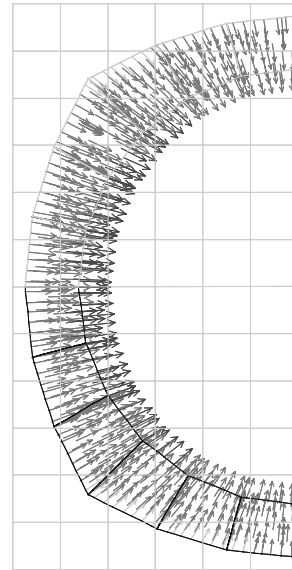
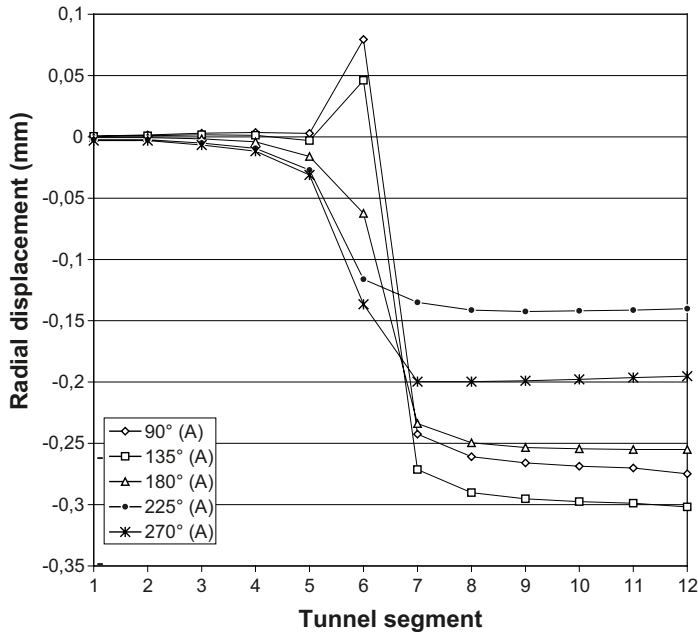


Figure 4-2. Displacements during excavation (drift segment numbers as in Figure 3-7), where 90° corresponds to drift roof and 270° to drift floor (left) and post excavation displacements on the drift perimeter (right).

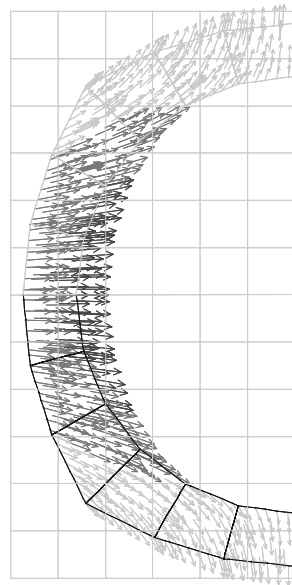
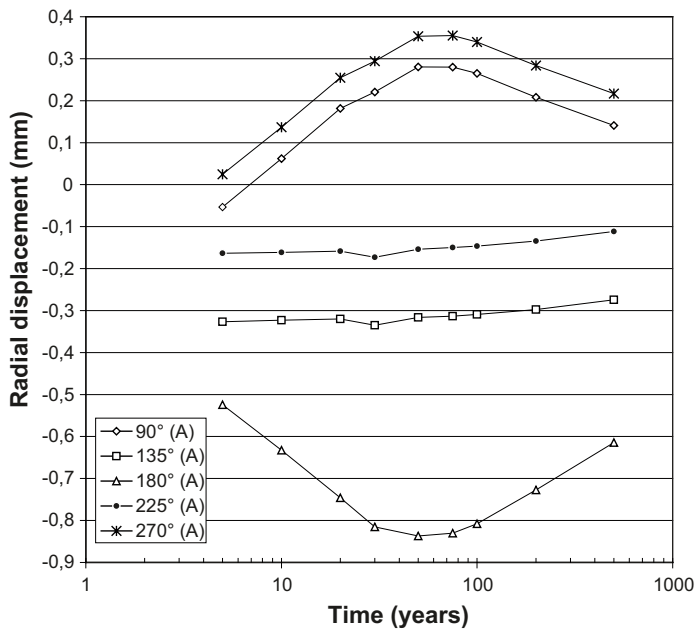


Figure 4-3. Displacements during the heating phase (left) and after 50 years on the drift perimeter.

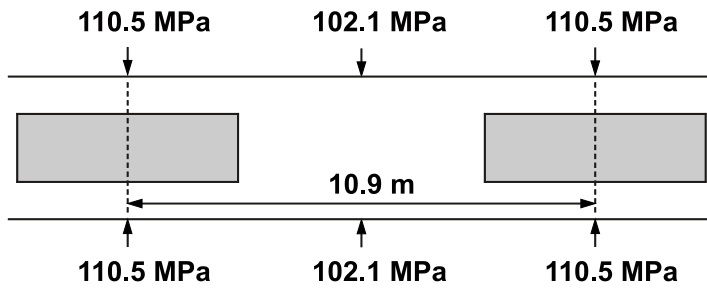


Figure 4-4. Maximum principal stresses (after 50 years) with position along drift (vertical section).

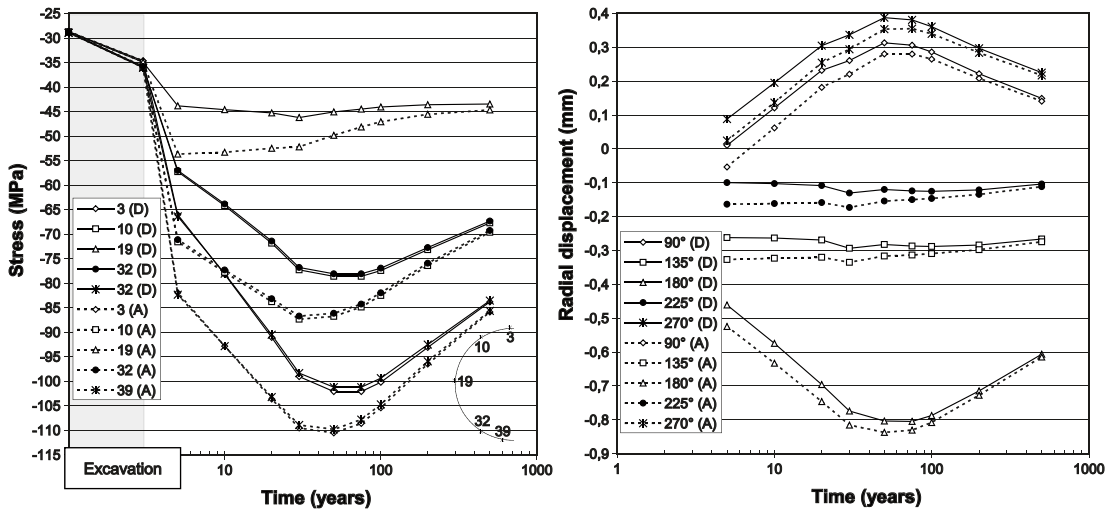


Figure 4-5. Principal stresses (left) and displacements (right) between canister positions (D). Grey shaded area represents non-thermal phase (primary equilibrium and excavation).

4.2 Relevance of boundary conditions

Using roller boundaries on all vertical sides of the model overestimates stresses particularly for longer times (by approximately 10 MPa). This shows that, although the horizontal boundary movements are small (see Figure 3-5 and Figure 4-6), they cannot be ignored.

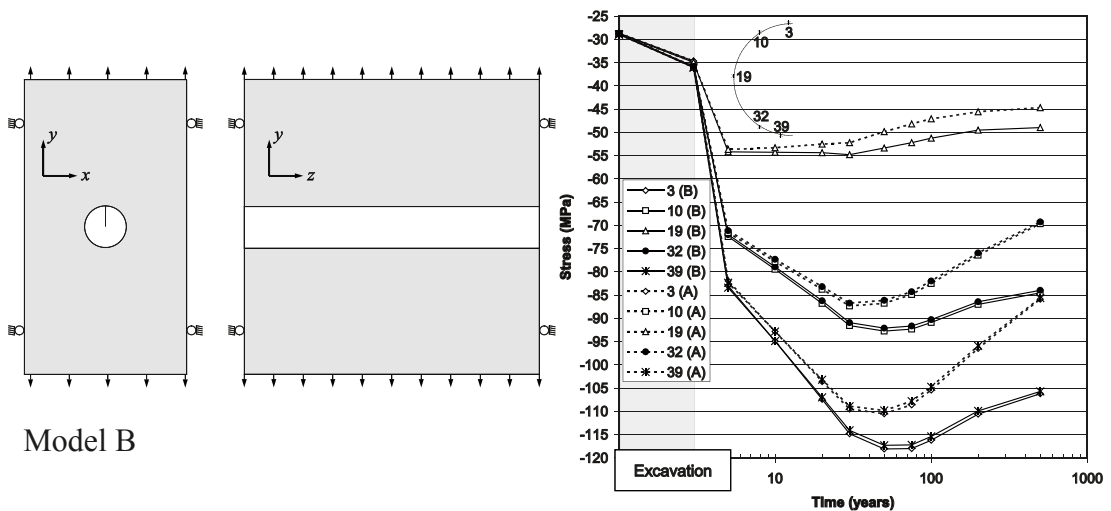


Figure 4-6. Vertically fixed in normal direction (Model B) vs. expanding boundaries (base case = Model A). Grey shaded area represents non-thermal phase (primary equilibrium and excavation).

4.3 Stress field

As there is an amount of uncertainty in the stress data for the models, we present a number of cases to determine how much effect these varied initial conditions will have on the major principal stress on the drift perimeter.

4.3.1 Stress magnitudes

As seen in Figure 4-7, using the lower stress magnitudes from Table 3-3 reduces the largest stresses by 16 MPa compared with the base case.

4.3.2 Stress orientation

Two cases with perfect symmetry about the co-ordinate axes are presented:

- σ_1 is along the drift, *i.e.* $\sigma_1 = \sigma_{zz}$, $\sigma_2 = \sigma_{xx}$ and $\sigma_3 = \sigma_{yy}$ ($\sigma_{xy} = \sigma_{xz} = \sigma_{yz} = 0$). Models F and I.
- Perfect symmetry, but σ_2 is along the drift, *i.e.* $\sigma_1 = \sigma_{xx}$, $\sigma_2 = \sigma_{zz}$ and $\sigma_3 = \sigma_{yy}$. Model G.

Model G is a “worst case scenario”, which can be avoided by aligning the deposition drifts with the major principal *in situ* stress.

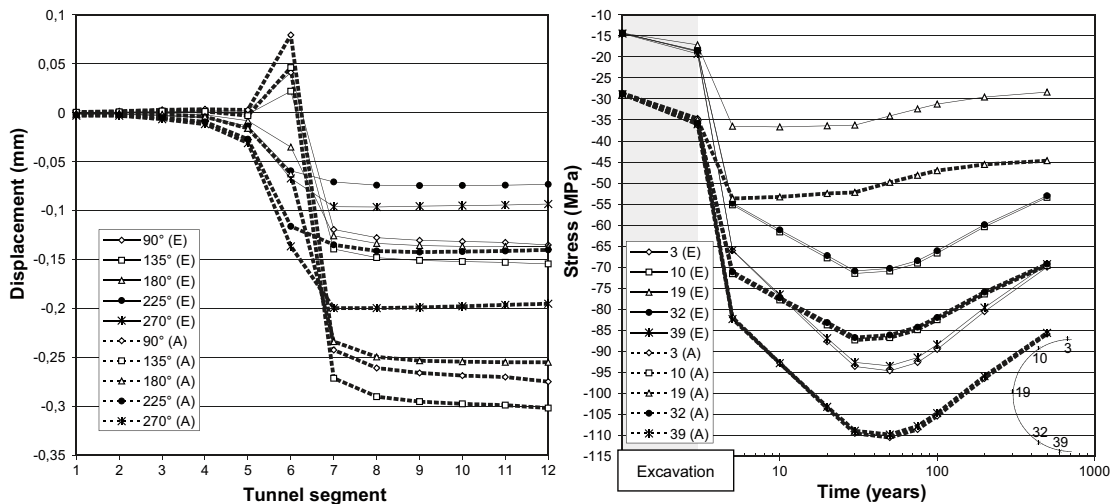


Figure 4-7. Lower limit *in situ* stress magnitudes (E). Displacements during excavation (left) and major principal stresses (right). Grey shaded area represents non-thermal phase (primary equilibrium and excavation).

As there is only a small change in *in situ* conditions (between the base case and having the principal stresses oriented along the model axes) the largest resulting principal stresses are increased by about 2 MPa, which can be seen in Figure 4-8.

As seen in Figure 4-9 the model with a vertical stress boundary (I) reproduces the results from the model with expanding/contracting boundaries on all sides (F).

Rotating the *in situ* stress tensor by 90° such that the major principal stress is oriented across the drift is the most unfavourable stress orientation. This arrangement increases the largest post-excavation stress significantly and hence also the stresses during the subsequent thermal phase. As seen in Figure 4-10 the largest stress is increased by 40 MPa compared with the base case.

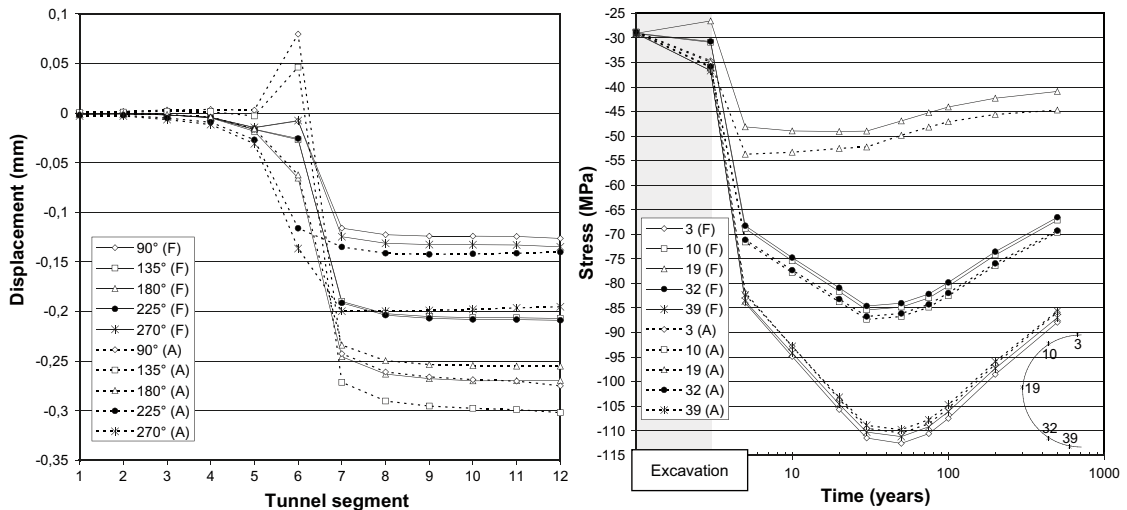


Figure 4-8. Perfect symmetry: σ_1 is parallel to the drift (F). Displacements during excavation (left) and major principal stresses (right). Grey shaded area represents non-thermal phase (primary equilibrium and excavation).

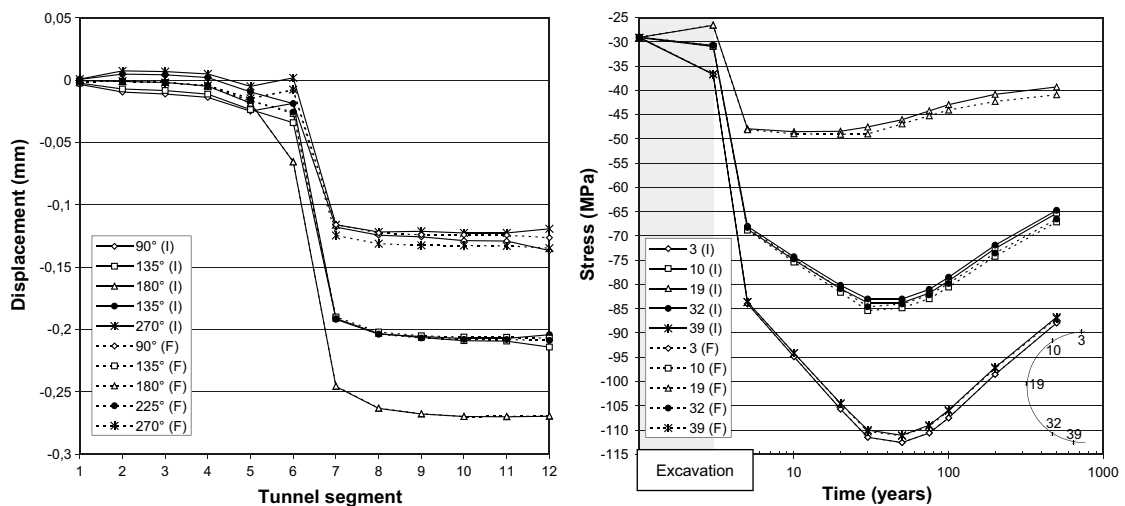


Figure 4-9. Expanding/contracting boundaries (F) vs. vertical stress on top (I). Displacements during excavation (left) and major principal stresses (right). Grey shaded area represents non-thermal phase (primary equilibrium and excavation).

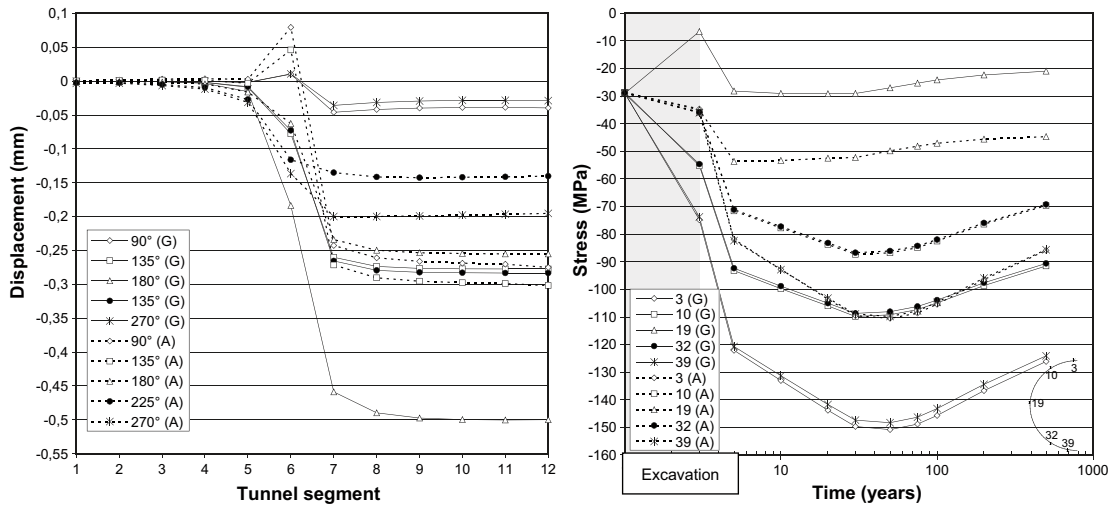


Figure 4-10. Perfect symmetry: σ_2 is parallel to the drift (G). Displacements during excavation (left) and major principal stresses (right). Grey shaded area represents non-thermal phase (primary equilibrium and excavation).

4.4 Influence of joint and internal drift pressure

Figure 4-11 shows that having a joint intersecting the drift results in negligible changes in the largest principal stress for case A *in situ* conditions.

Figure 4-12 shows tangential stresses on the drift perimeter with given internal drift pressures compared with the base case. For pressures below 25 MPa the tangential stress decreases with increasing internal drift pressure at all positions as expected. However, for internal pressures greater than 20 MPa the zero fracture tensile strength prevents the stresses from becoming tensile at 180°.

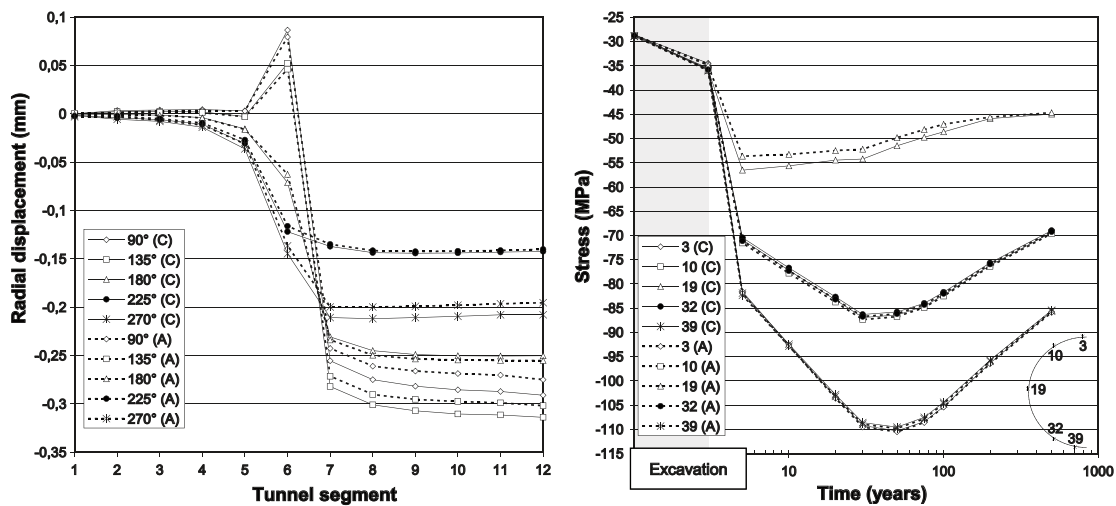


Figure 4-11. One horizontal joint. Displacements during excavation (left) and major principal stresses (right). Grey shaded area represents non-thermal phase (primary equilibrium and excavation).

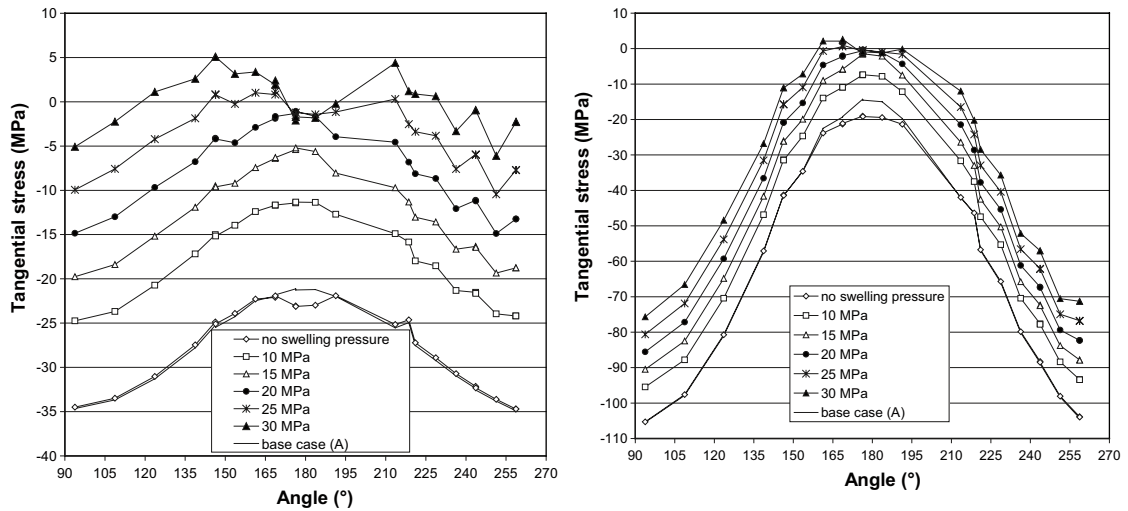


Figure 4-12. Tangential stresses on drift perimeter after excavation (left) and after 100 years heating (right).

Figure 4-13 shows normal joint displacements following internal pressure increases directly after excavation, including the effects of excavation. The resulting opening depth from internal pressures greater than or equal to 15 MPa applied after excavation will open the joint to its entire length.

Figure 4-14 shows normal joint displacements following internal pressure increases after 100 years of heating, including the effects of excavation. After 100 years of heating, applying internal pressures of 30 MPa or less will result in an opening depth less than one metre.

Here, a constant value of JKN has been used throughout (cf Figure 3-2). The selected value is relevant for fractures in low compression. This means that the largest joint normal openings close to the drift wall are well estimated. Closure is overestimated. The point of transition from opening to closure, however, is independent of the stiffness model.

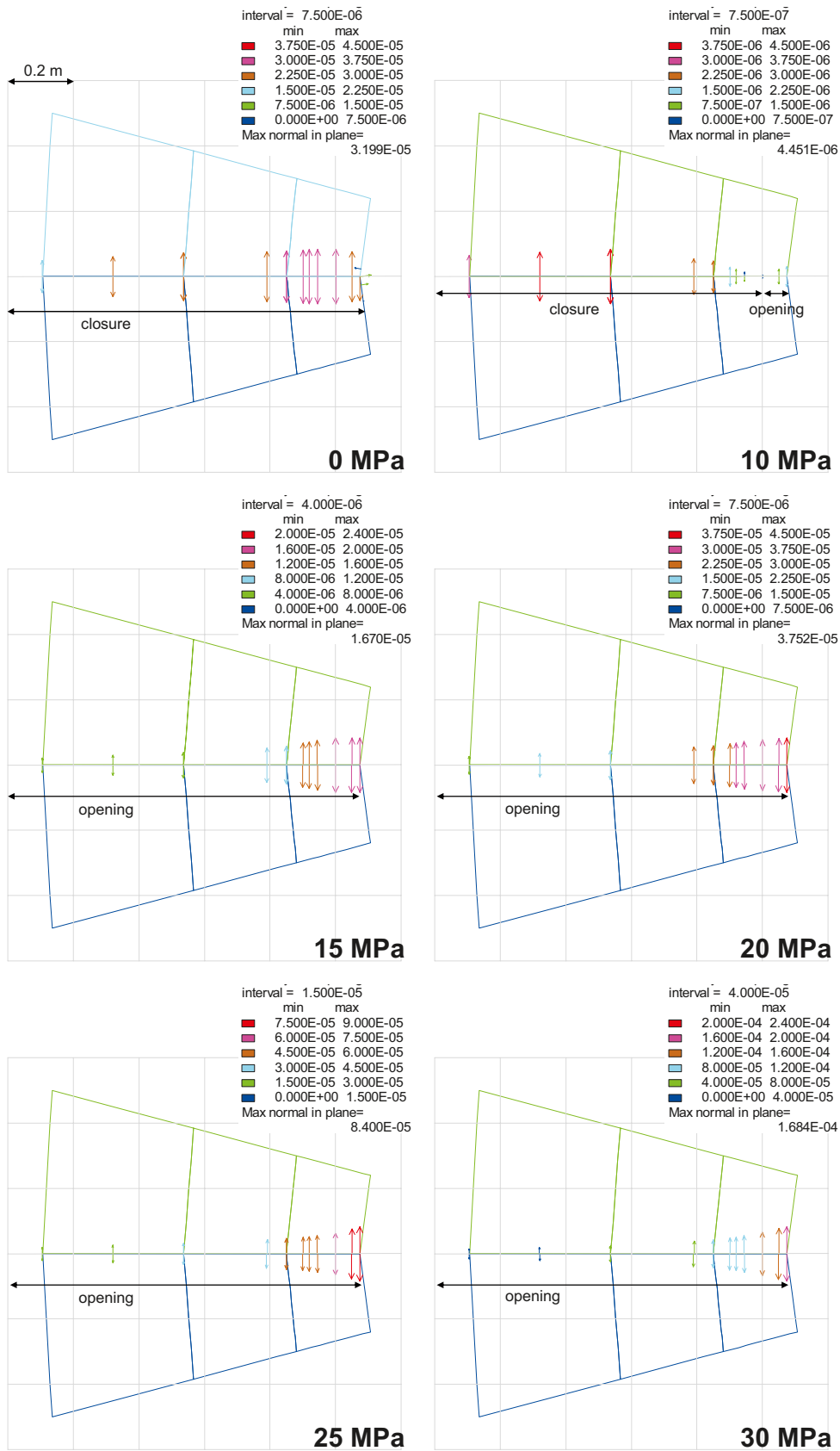


Figure 4-13. Normal displacement of joint after excavation and application of given swelling pressures.

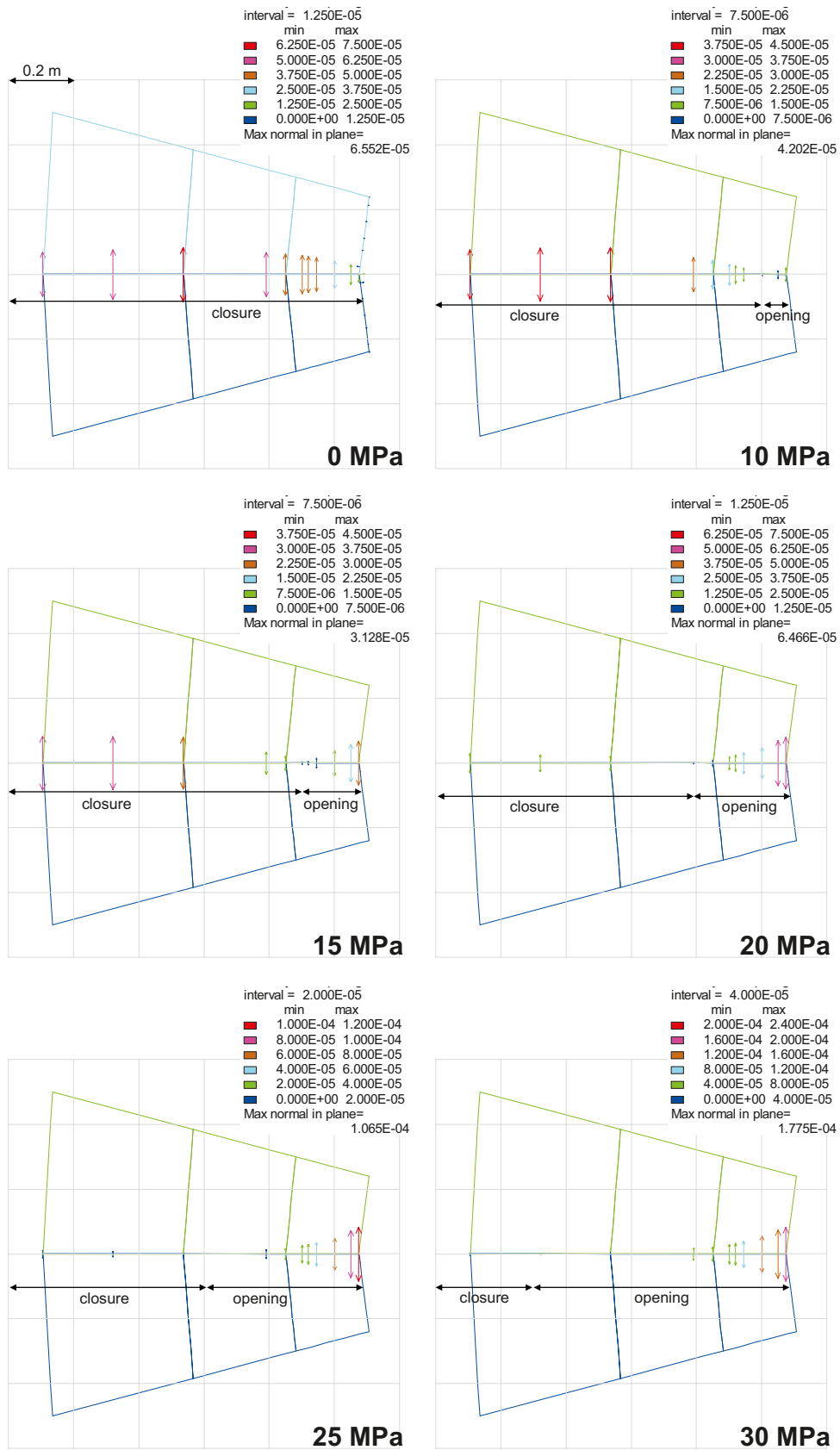


Figure 4-14. Normal displacement of joint after excavation, 100 years heating and application of given swelling pressures.

5 Result, summary and discussion

5.1 General

There are two major concerns regarding stresses on the KBS-3H drift perimeter:

- As a result of excavation and subsequent heating, tangential stresses in the floor and roof will be high. If the stresses approach and exceed the crack initiation stress σ_{CI} (which makes out 45–50% of the intact rock uniaxial compressive strength of the Olkiluoto rock types /Posiva 2007/, there is a risk of spalling in these parts of the rock.
- The other concern is that normal stresses on horizontal joints running parallel with the drift and intersecting at drift mid-height will remain low (or even decrease for certain *in situ* stress states) after excavation. With the addition of an internal drift pressure due to swelling buffer materials or gas development the normal stress will be further reduced.

Taking the crack initiation stress σ_{CI} as a measure of the spalling strength, the spalling strength of the Olkiluoto rock types ranges between 52 and 59 MPa /Posiva 2007/.

Figure 5-1 shows the principles. Both potential problems are more pronounced if the anisotropy of the remote stress state is high. Internal drift pressures decrease the spalling risk and increase the opening risk.

5.2 Excavation

5.2.1 Stresses along the perimeter

The tangential stress $\sigma_{\theta\theta}$ on the perimeter of the circular KBS-3H opening, subjected to a biaxial stress state with principal stresses p ($= \sigma_{yy}$ vertical) and pK ($= \sigma_{xx}$ across drift), can be obtained using the formula given by given by /Kirsch 1898/:

$$\sigma_{\theta\theta} = p[(1 + K) + 2(1 - K) \cos(2\theta)] \quad (5-1)$$

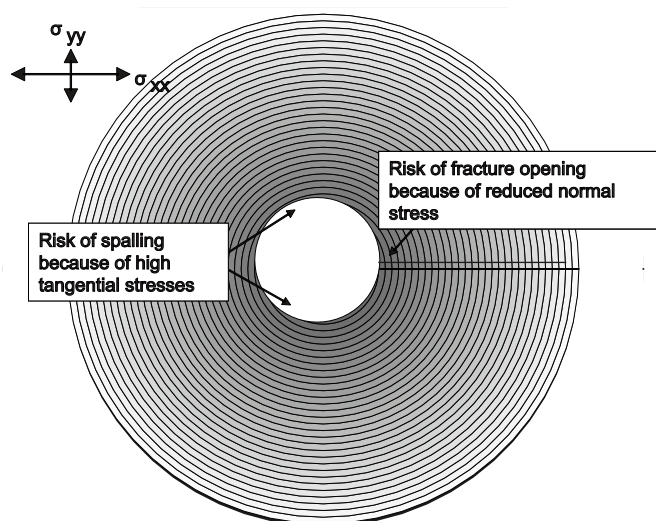


Figure 5-1. Concerns addressed in this study.

Figure 5-2 shows tangential and axial stresses (*in situ* axial stress, σ_{zz} , marked with a dot) on the drift perimeter as well as the major principal stress in a vertical cross section at model mid-length. The tangential stresses are represented well by 3DEC compared with the analytical solution due to Kirsch. Note that, for models with a sub-horizontal major principal *in situ* stress, the major principal stress (σ_1) on the drift perimeter coincides with the tangential stress only in the floor and roof areas. In the perfect symmetry models, σ_1 is either tangential or axial.

5.2.2 Spalling risk

The maximum tangential stresses on the drift perimeter range between 19 MPa (E) and 75 MPa (G) as seen in Figure 5-2. The uniaxial compressive strength (UCS) is in the range 108–122 MPa, *i.e.* average values for the different Olkiluoto rock types /Posiva 2007/. The strength of Olkiluoto gneissic rocks is dependent on the foliation angle and these values represent minimum values (foliation angle 30–60°) /Posiva 2007/. This means that the approach taken here is conservative. The crack initiation stress ranges between 52 MPa and 59 MPa /Posiva 2007/. Taking the crack initiation stress as a measure of the spalling strength, it does not seem likely that there will be significant spalling after excavation, unless drifts are oriented as in model G, *i.e.* with σ_1 normal to the drifts. The margin (to the lowest threshold) is in the range 15 to 33 MPa. For model G the lowest threshold (52 MPa) is exceeded by about 23 MPa, whereas the highest threshold is exceeded by about 16 MPa.

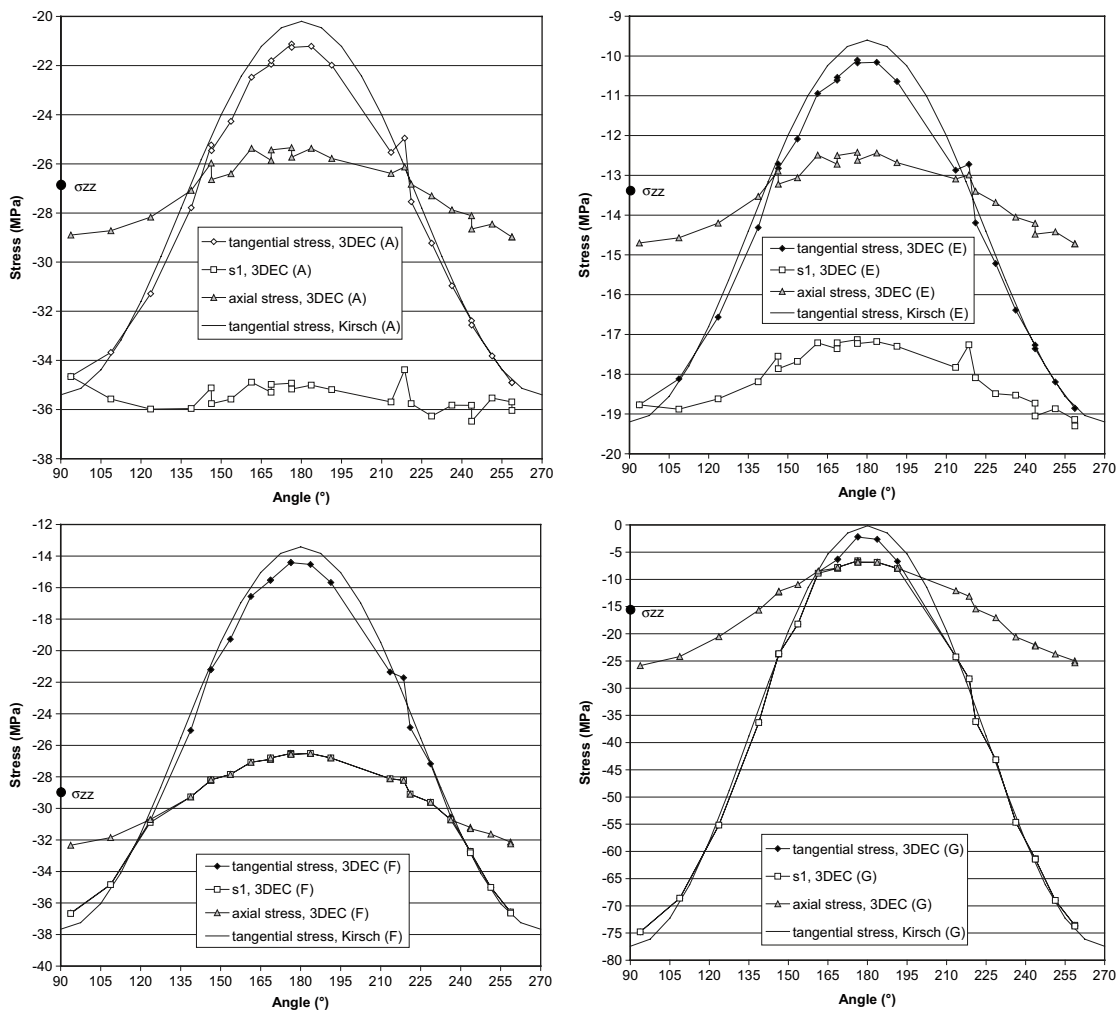


Figure 5-2. Post excavation stresses on the drift perimeter (90° corresponds to drift roof and 270° to drift floor).

5.2.3 Reactivation (opening) risk

Unsupported drift

Similar to the spalling risk, the risk of fracture opening can be assessed by considering the periphery stresses. Fractures with orientation and location as indicated in Figure 3-6 (left) are the most sensitive ones. If the tangential springline ($\theta = 180^\circ$) compressive stress decreases below the initial fracture normal stress, that fracture will open. As long as the tensile strength is not exceeded, the aperture increase will be controlled by the joint normal stiffness. Fractures with zero tensile strength (as assumed here) will fail in tension if the compression drops below zero. Looking at Figure 5-2, we find that the fracture will open for case G (initial fracture normal stress 9.74 MPa, cf Table 3-3) as result of excavation. For Case E (initial fracture normal stress 6 MPa) and F (initial fracture normal stress 9.74), the fracture is close to opening as a result of excavation. For Case A (initial fracture normal stress 12 MPa) the fracture closes.

Internal drift pressure

The tangential stress at radial distance r from the centre of a long cylindrical opening (provided that the medium is elastic) of radius a and with internal pressure p_I can be derived from /Timoshenko and Goodier 1970/:

$$\sigma_{\theta\theta} = p_I \frac{a^2}{r^2} \quad (5-2)$$

Adding this expression to the more general form of Kirsch's solution (below) gives the total normal stress (*i.e.* effects of excavation and internal pressure) on a radial joint, such as the horizontal one considered here, a distance r away from the drift centre.

$$\sigma_{\theta\theta} = \frac{p}{2} \left[(1 + K) \left(1 + \frac{a^2}{r^2} \right) + (1 - K) \left(1 + 3 \frac{a^4}{r^4} \right) \right] \quad (5-3)$$

Here, p , K and a are defined as above.

Figure 5-3 shows analytically calculated normal stresses on the horizontal joint for the four different stress cases. It can be seen in the figure that swelling pressures greater than or equal to 10 MPa will be enough to open the joint in the base case (A). However, a swelling pressure of 10 MPa will only open the joint 0.1–0.2 m from the drift perimeter, whereas swelling pressures greater than or equal to 15 MPa will open the joint to very large depths. There will be potential tensile failure to a depth of 12 cm for an internal pressure of 25 MPa. The corresponding depth for an internal pressure of 30 MPa is 25 cm. Cases E, F and G (cf Figure 5-2) are subjected to lower normal stresses on the joint than the base case which means that even lower pressures than 10 MPa will be sufficient to open the joint. This is also clear from Figure 5-3.

Figure 5-4 shows a comparison between the analytical solution due to Kirsch (equation 5-3) and 3DEC for the unsupported drift case, *i.e.* a verification of the 0 MPa curve in Figure 5-3. As seen in the figure the two solutions agree within approximately 1 MPa. The noise in the 3DEC results is due to irregular finite difference mesh, which gives zone centroids that are not necessarily located exactly on the scan-line.

Figure 5-5 shows joint normal displacements for the base case stress orientation/magnitude (model C) compared with analytical estimates, where the analytical expression is given by:

$$\Delta u = \frac{\text{change in stress}}{JKN} \quad (5-4)$$

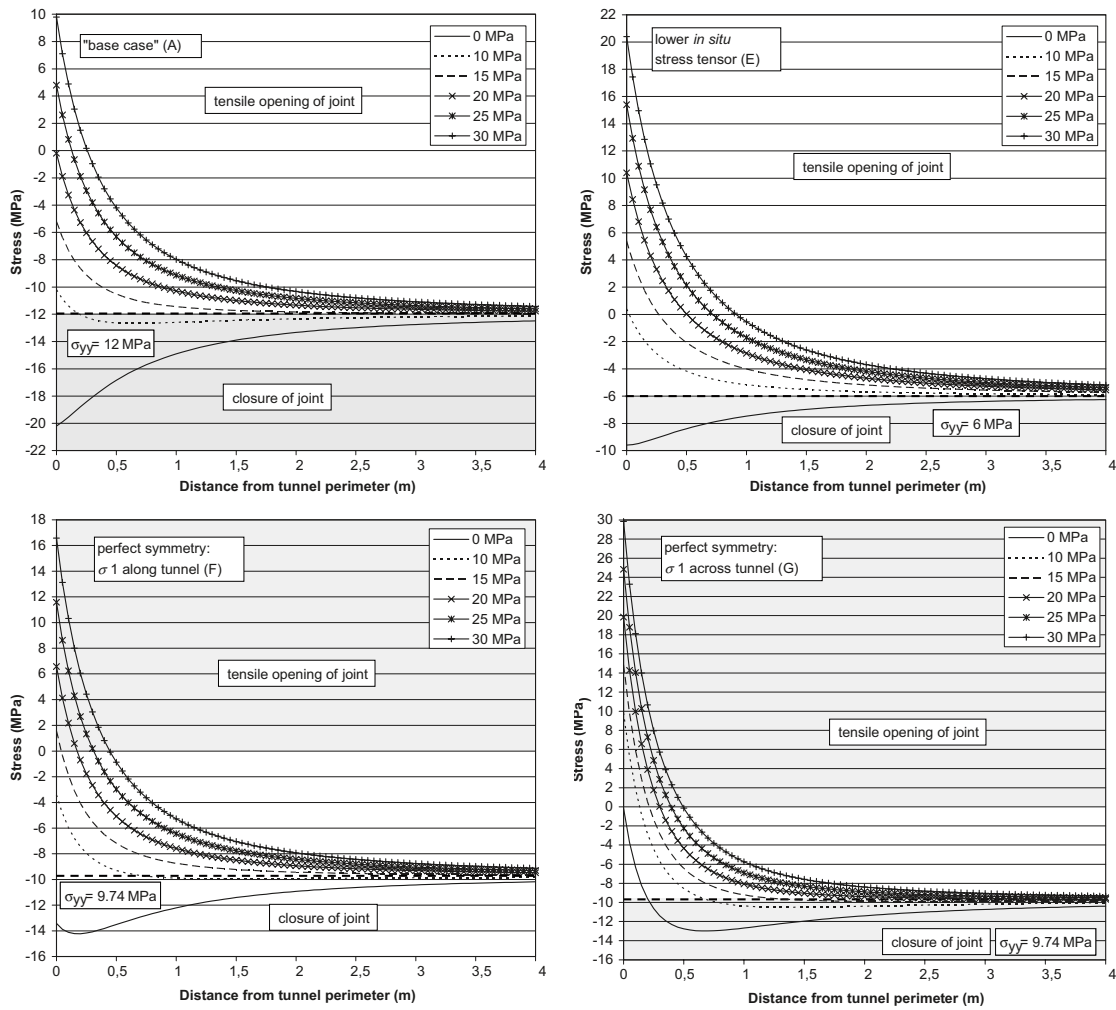


Figure 5-3. Normal stress on horizontal joint. The opening threshold is given by the in situ vertical stress σ_{yy} .

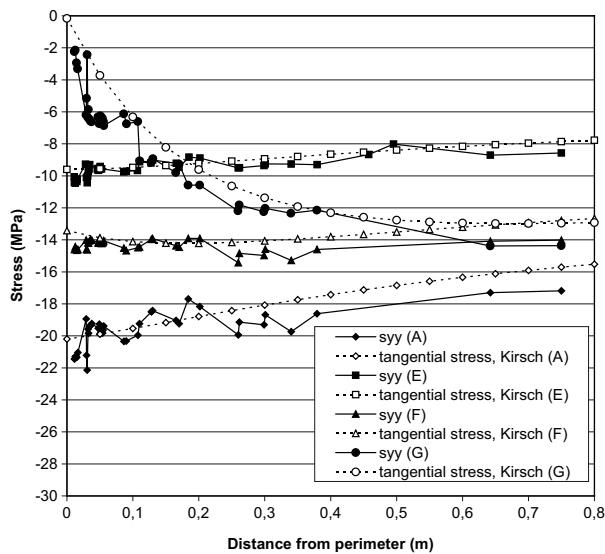


Figure 5-4. Normal stress on horizontal joint with no internal drift pressure. Comparison between analytical expression (Kirsch, eqn 5-3) and 3DEC.

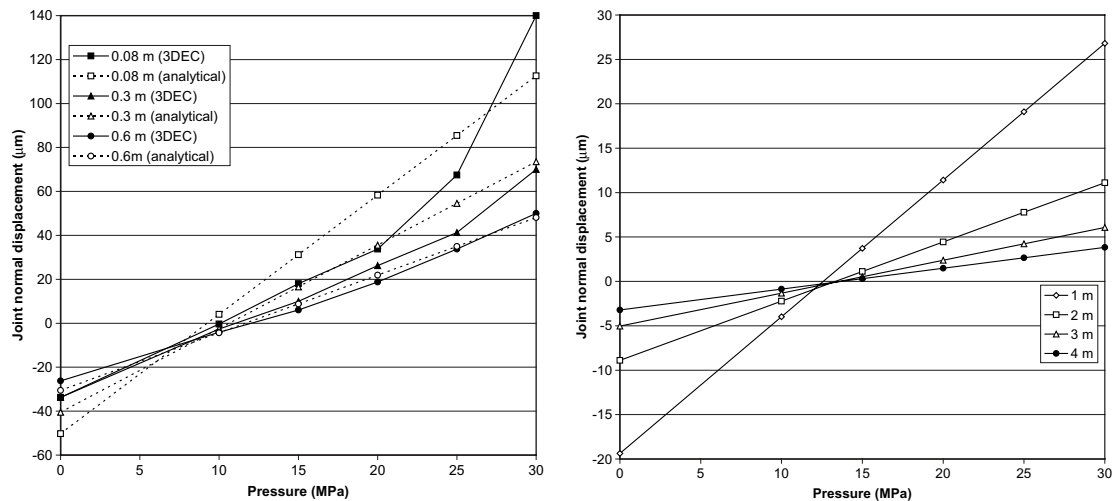


Figure 5-5. Joint normal displacements, due to excavation, at given distances from the perimeter as functions of internal drift pressure. Near-field comparison of equation 5-4 with 3DEC (left) and analytical “far field” estimates (right).

Equations 5-2 and 5-3 above with the vertical *in situ* stress (12 MPa) subtracted give the change in stress. The joint normal stiffness, $JKN = 150 \text{ GPa/m}$ is given in Table 3-2.

Note that the values in Figure 5-5 are taken directly from the 3DEC plots in Figure 4-13 and are somewhat approximate. The large discrepancies between the results for the 0.08 m curves, for pressures greater than 25 MPa, are due to the fact that 3DEC accommodates for tensile failure, whereas the analytical expression does not. The depth of tensile failure, for given internal pressures, can also be seen in Figure 5-3 (top left).

5.3 Thermal phase

5.3.1 Thermal disturbance – general

Displacements

At the time of maximum displacement (between 50 and 75 years after deposition), the drift in the base case has contracted 0.85 mm horizontally across the drift and expanded 0.3 mm vertically at both floor and roof (cf Figure 4-3). As seen in Figure 5-6, 0.6 mm of the horizontal contraction is due to heating phase alone. Another observation is that the vertical expansion of the drift floor and roof is 0.55 mm (not taking into account the contraction due to excavation).

Stresses

Figure 5-7 shows purely thermal stress contribution, *i.e.* the stress additions induced by heating, on the drift perimeter. For models with the same heat load, thermo-mechanical properties and boundary conditions, these stress additions will be the same, provided that the inelastic deformations (if any) are small. In the present study, all models are fully elastic at all times, with the exception of the drift pressure models, where tensile failure was found nearest the drift at the highest drift pressures. Therefore, adding these results to the post-excavation tangential stresses in Figure 5-2 would give the total tangential stresses on the drift perimeter for all other cases, irrespective of *in situ* stress directions and magnitudes. The largest tangential thermal stress additions are found near the floor and roof of the deposition drift. These stress additions amount to approximately 76 MPa after 50 years (see Figure 5-7) and would apply for all models, irrespective of the initial stress state.

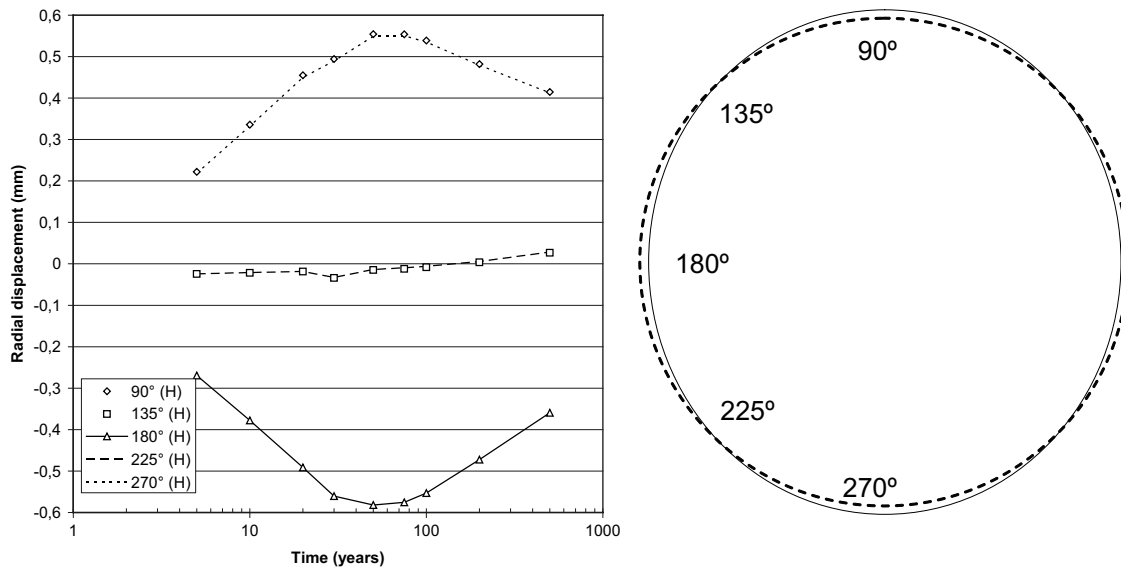


Figure 5-6. Thermal displacements – no in situ stresses present. Outward displacements are positive. Right shows deformed drift section schematically compared with original shape (dashed).

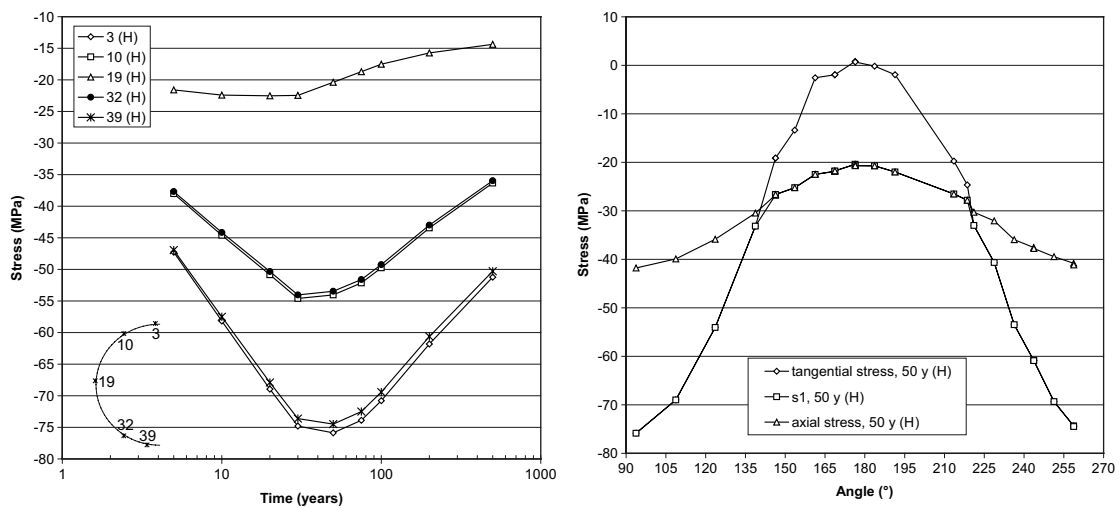


Figure 5-7. Major principal stresses (left) and stress distribution along the drift perimeter (right, cf. Figure 2-7 middle left).

Boundary conditions

Although the movements of the horizontal boundaries are small (see Figure 3-5) they cannot be ignored. As seen in Figure 4-6 this would overestimate the tangential stresses by approximately 10 MPa at stress maximum (50 years). Note that we have applied expansion/contraction histories obtained from the analytical solution that are based on the assumption of a homogenous, linear elastic rock mass. In reality soft fracture zones may absorb some of the thermal strain and allow for larger expansion of the nearfield rock at some places, which would reduce the thermal stresses further. The importance and the potential of this possibility remain to be explored.

5.3.2 Perimeter stresses after 50 years – different cases

As seen in Section 4 the largest major principal stresses reach their maxima after approximately 50 years. Figure 5-8 shows the stress distribution on the drift perimeter after 50 years heating for the near-field models in Section 4.

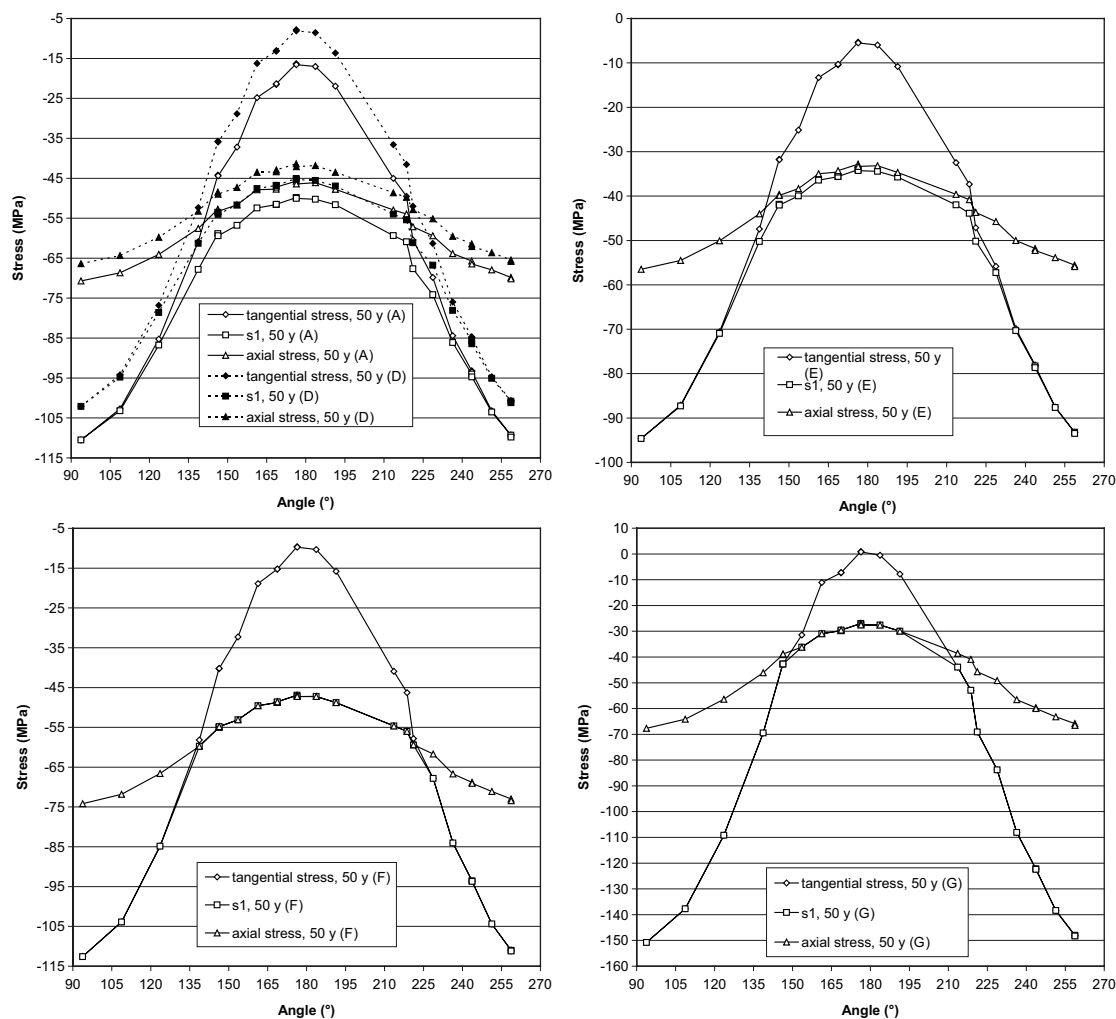


Figure 5-8. Tangential, axial and major principal stress on drift perimeter at the time of maximum stress (50 years).

5.3.3 Temporal evolution at some periphery points

Figure 5-9 (left) shows the time-evolution of the largest major principal stresses. The largest tangential stresses in the reference case (A) are approximately 110 MPa and found near the floor and roof of the drift. The largest tangential stress between two canister positions is 16 MPa lower than the corresponding stress for the base case after 5 years. This difference decreases steadily with time. At the time of maximum stress (50 years) the difference is 9 MPa and after 500 years it is only 2 MPa.

As models A, E, F and G have the same thermal load and boundary conditions their purely thermal stress contributions are identical (cf Figure 5-7). The following can be observed by varying the stress tensor in magnitude and direction (cf Figure 5-9):

- The lower limit stress tensor (see Table 3-3) gives a decrease in maximum tangential stress of 18 MPa (E compared with A).
- Assuming that the principal stresses are oriented along the axes (with σ_1 along the drift) gives a small increase in maximum tangential stress (approximately 2 MPa) (F compared with A).
- Rotating the stress tensor 90° horizontally, such that σ_1 is across the drift, gives an increase in the maximum tangential stress of 40 MPa (G compared with A). However, case G is unlikely to occur since it can be avoided by aligning the drifts with the major principal stress.

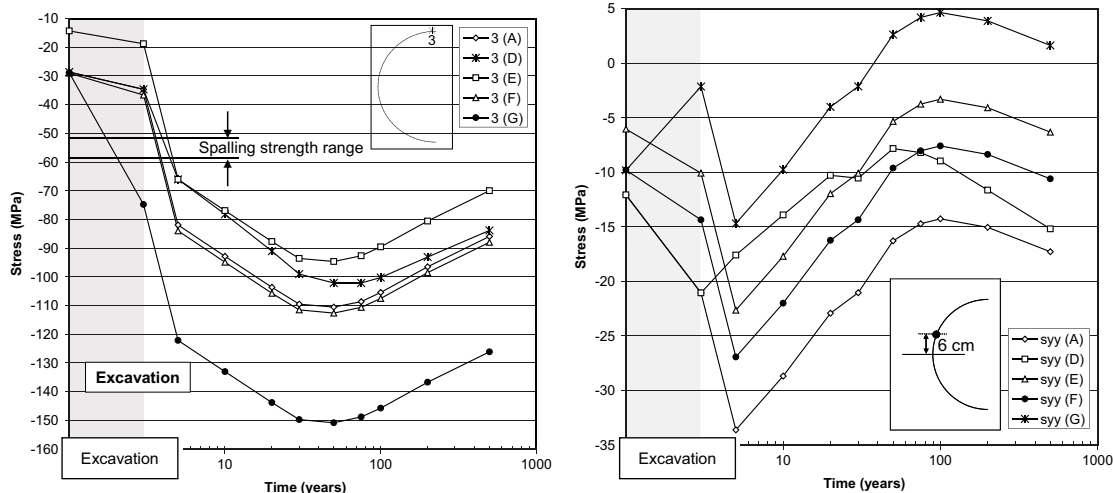


Figure 5-9. Largest principal stress on drift perimeter (left) and smallest vertical stress (right). Grey-shaded areas represent pre-thermal stresses, i.e. *in situ* stresses and stresses due to excavation. First thermal stress analysis after 5 years.

It is also clear from Figure 5-9 (left) that the spalling threshold (52–59 MPa) is not exceeded after excavation for any other case than G, and that this threshold is exceeded for all cases already after 5 years of heating.

Figure 5-9 (right) shows the time-evolution of the vertical stress on the horizontal joint. During the first few years after deposition, the stresses increase and reach their maximum value some time before 10 years. Thereafter they decrease and reach their minima after approximately 100 years. In all models this minimum is less than the post-excavation vertical stress and also (with the exception of the base case) less than the initial *in situ* vertical stress.

5.3.4 Spalling risk

The thermal load generates sufficiently high periphery stresses that the spalling threshold ($=\sigma_{ci}$) will be well exceeded in the floor and roof regions, irrespective of the initial stress state. After 50 years the thermal stress addition alone (about 75 MPa) makes out 60–70% of the uniaxial compressive strength and exceeds the spalling strength by between 16 and 23 MPa. In dry drift sections without supporting pressure from swelling bentonite, spalling is consequently almost certain to occur.

The effect of the swelling pressure is to suppress initiation and progression of the brittle failure rather than to bring about substantial changes in the stress state.

Therefore, swelling pressures much too low to bring the maximum stress below the spalling threshold may be sufficient to prevent spalling /Cho et al. 2002/.

5.3.5 Reactivation (opening) risk

Figure 5-9 (right) shows the vertical stress on the horizontal joint for the different stress orientations and magnitudes. Due to zone length the nearest zone sufficiently close to the drift perimeter is 6 cm above the joint.

Unsupported drift

As a result of the heating the normal stress on the joint, in models D, E, F and G, will decrease below the vertical *in situ* stress after between 10 and 50 years (cf Figure 5-9, right). In model A, an internal pressure of 2–3 MPa will be sufficient to open the joint, compared with its initial pre-mining aperture. Model G is in tensile failure by heating alone (*i.e.* without any internal drift pressure).

Internal drift pressure effects

As stated above, in all models (with the exception of the base case) compression on the joint will decrease sufficiently to open it, compared with the initial pre-mining aperture, regardless of internal pressure (cf Figure 5-8 (drift mid-height, 180°) and Figure 5-9 (right)). These models will reach tension (and possibly tensile failure) if internal pressures of the order 8 MPa (model D), 3 MPa (model E) and 7–8 MPa (model F) are applied. As stated above, model G is already in tensile failure (given that the fracture tensile strength is zero). Swelling pressures of as little as 2–3 MPa will be sufficient to open the joint in model A (about 15 MPa is needed to bring it to tensile failure).

Figure 5-10 shows a semi-analytical estimate of the vertical stress a radial distance r from the drift perimeter. The stress contributions due to excavation and internal pressure are given by equations 5-2 and 5-3 above, whereas the purely thermal stress contribution (numerical 3DEC results) is given by model H.

Figure 5-11 shows a comparison of internal pressure effects after excavation (or after the temperatures have returned to their initial undisturbed values some 50,000 years after excavation) and the pressure effects after 100 years of heating. The thermal stresses suppress the tendency to open at distances larger than about 0.1 m from the periphery, whereas they promote opening close to the periphery. This picture is not constant over time, however:

- at early times thermal stresses are localized to the nearest surrounding, giving increased compression at the periphery (cf Figure 5-9, right).
- at later times the thermal stresses will effectively appear as additions to the *in situ* stresses and increase the stress anisotropy. This will contribute to reduce the compression close to the periphery (as seen here), cf Figure 5-9, right.

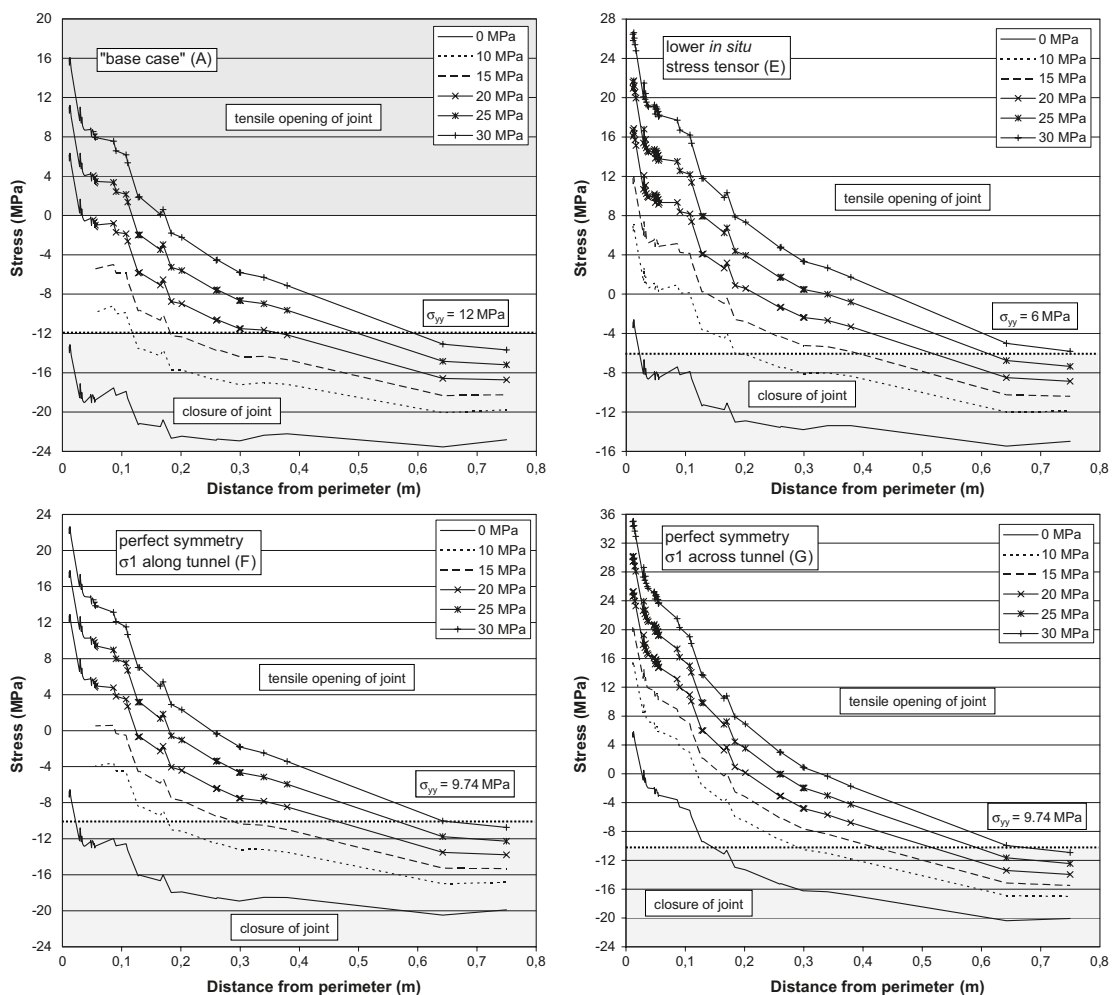


Figure 5-10. Normal stress on horizontal joint after 100 years.

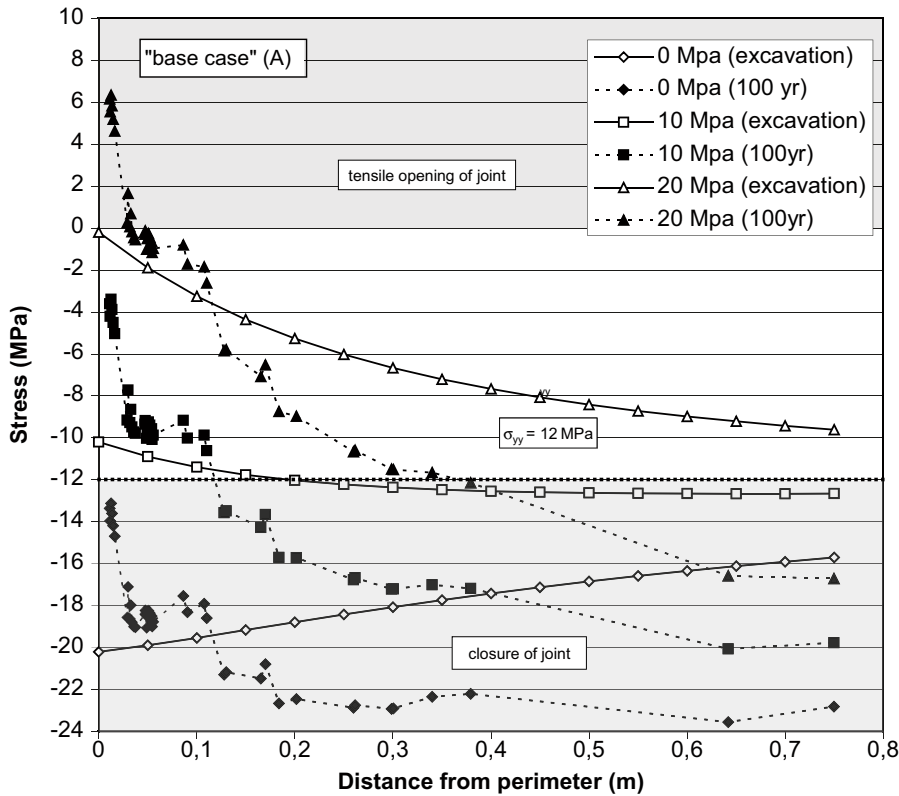


Figure 5-11. Base Case. Comparison between effects of internal drift pressure after excavation and after 100 years of heating. The intersection with the 12 MPa level indicates the depth of opening.

Figure 5-12 (left) shows the joint normal displacements (for model C, base case *in situ* stresses and active horizontal joint) after 100 years heating compared with the corresponding displacements due to excavation. The right part of the figure shows the joint's opening depth. As before, the values for the joint normal displacements are taken from the 3DEC plots in Figure 4-14 and are somewhat approximate. Note that the results agree with those shown for 10 MPa and 20 MPa in Figure 5-11.

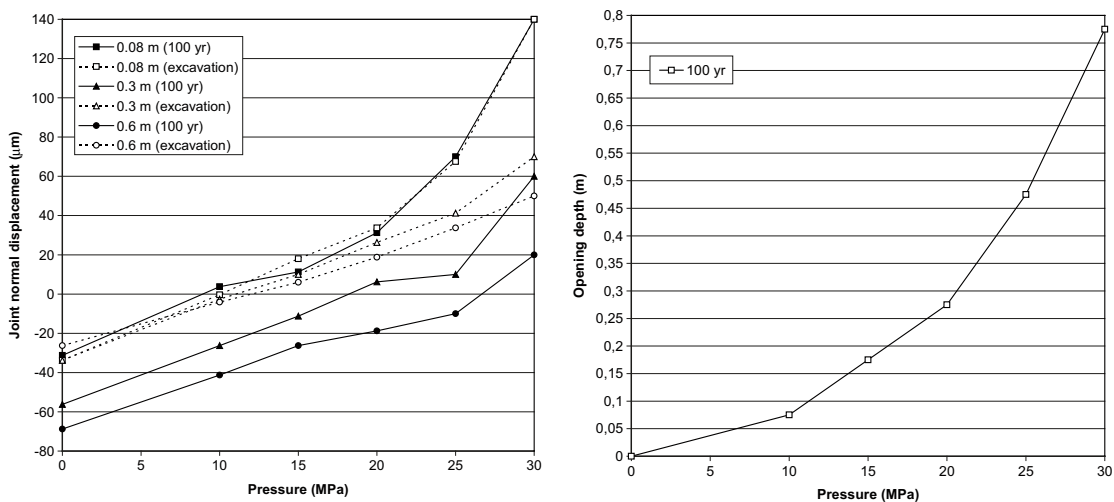


Figure 5-12. Joint normal displacements at given distances from the perimeter as functions of internal drift pressure. Comparison between 100 years heating and excavation (left). Opening depth (right).

6 Summary

6.1 General

There are two major concerns regarding stresses on the KBS-3H drift perimeter:

- The risk of spalling in highly stressed unsupported parts of the deposition drift, *i.e.* the floor and roof areas.
- The risk of opening of horizontally intersecting fractures due to decreased vertical compression.

The two concerns are analyzed here by use of 3DEC near-field models. The mechanical and thermo-mechanical effects of the entire repository were included by defining the near-field model boundary conditions as to account for the repository- scale, time-dependent stresses and displacements.

Four different *in situ* stress states were considered, each corresponding to a separate 3DEC model (A, E, F, G). The base case stress state (A) was defined to agree with the stress data (upper limit values) and the drift orientation given for the Olkiluoto site. The other models were analyzed to examine the sensitivity of the results to *in situ* stress magnitude (E) and orientation (F,G).

One additional model was analyzed to examine the base case conditions between canisters (D) rather than at canister mid-length, and one additional model to find and single out the thermal stress additions (H). Other models were analyzed to demonstrate the validity and consistency of the boundary condition approach (B, I).

One particular base case model version (C) was analyzed with an explicitly modelled fracture. For analyzing the response of the fracture, it is however not necessary to model it explicitly unless the inelastic components of the deformations are significant. In the models analyzed here this was not the case, meaning that the elastic models can be used with good accuracy also to examine the fracture opening issue.

6.2 Spalling

Significant spalling after excavation is found to be unlikely if the drifts are sub-parallel to the major stress. For the Olkiluoto rock types, the crack initiation stress σ_{CI} ranges between 52 and 59 MPa /Posiva 2007/. The lowest value applies for the main rock type (veined gneiss). Taking σ_{CI} as a measure of the spalling strength, which is a somewhat conservative assumption, the margin to the lowest threshold is found to be 15–33 MPa. If the drifts would be oriented perpendicularly to the major stress, however, spalling is almost certain to occur. The 52 MPa spalling threshold would be exceeded by about 23 MPa, while the highest (59 MPa) would be exceeded by about 16 MPa. This is however a hypothetical worst case orientation that will be avoided in the layout work. In principle it would be possible to find (using the analytical tools described here) the maximum angle between major stress and drift axis that should be allowed to keep the maximum periphery stress below the spalling threshold.

Spalling after a few years of heating is almost certain to occur if there is no supporting pressure from the drift buffer. After 50 years of heating, the thermal stress additions alone (*i.e.* without inclusion of any secondary stresses generated by excavation in the *in situ* stress field) are more than sufficient to push the roof and floor stresses over the spalling threshold. The maximum total stress at that time may even be on level with the uniaxial compressive stress reported for the Olkiluoto veined gneiss. The question of the internal drift pressure required to suppress initiation and progression of stress-induced failures was not addressed here. However, it has been estimated that pressures of the order from 150 to 200 kPa could be sufficient /SKB 2006b, Posiva 2006/.

6.3 Fracture opening

Fracture opening, assuming fracture properties described in Table 3-2, will occur if the fracture normal stress is reduced in comparison to pre-mining conditions. If the resulting normal stress drops to zero, the fracture is likely to fail in tension. In the elastic range the fracture opening is determined by the joint normal stiffness.

It was found that excavation increases the fracture normal stress in all cases and at all distances from the periphery except for the case with the major stress being perpendicular to the drift (G). In case G the fracture will open close to the periphery but not at distances larger than about 0.25 m. The fracture does not fail in tension anywhere, though.

The effect of internal drift pressures is to reduce the fracture normal stresses further. Without any thermal load, the fracture will open to large depths if the pressure exceeds the vertical *in situ* stress. However, at some distance from the drift that opening is very minor: 12 μm for the 20 MPa pressure at 1 m distance and about 2 μm at 4 m distance. The thermal load reduces the opening depth, however with different amounts at different times.

None of the models gave tensile failures at larger depths than 1 m (30 MPa drift pressure, no heat, low stress model). For the base case the maximum depth of tension is about 0.2 m from the periphery.

6.4 Relevance and validity, future work

All 3DEC models were analyzed assuming practically fracture-free rock. Slip along numerous fractures of different dip and strike might have changed some of the results. At some places there would be local stress concentrations and in other stress relaxations. However, experience is that fracture slip in rock in compression, such as at 400 m depth at the Olkiluoto site, would not change the general picture much /Hökmark et al. 2006/. Nevertheless, models with base case stresses and with realistic fracture populations and with realistic values of fracture property parameters should be analyzed to verify this.

The large-scale thermo-mechanical behaviour was assessed by use of analytical solutions based on the assumption of linear heat conduction in an isotropic, homogeneous and linearly elastic medium. Large-scale numerical models should be analyzed to explore the importance of fracture zones between, above and below the panels. Potentially, some of the large-scale thermal strain would be absorbed, giving more volume expansion during the heated phase. Looking at the high tangential stresses after 100 years, it seems unlikely, however, that this would change the general conclusion, *i.e.* that there will almost certainly be spalling in dry, unsupported drifts.

The near-field models were assumed to be located in the central parts of a deposition panel. It has been shown that the differences between different panels are small. In that sense, the model results are representative of the repository as a whole. Additionally it should be examined if there are significant differences in positions close to panel edges and panel corners.

Opening estimates are based on a simplified stress-closure model with a fixed value of the joint normal stiffness. In reality, the joint normal stiffness depends on the normal stress, giving smaller values of opening/closure for fractures in high compression.

Swelling pressure and gas pressure were represented here as pressure on the drift walls. Effects of gas pressures in the fractures, or of gas movement, were not considered.

All spalling risk estimates were made using the crack initiation stress as a measure of the spalling strength. This is a conservative assumption. /Martin 2005/ suggests that the spalling strength should correspond to about 55% of the uniaxial compressive strength. This means that the spalling strength may have been underestimated by 7–8 MPa. However, applying the 55% threshold would not change the general conclusion, *i.e.* that there will be no spalling during construction, but almost certainly after sometime of heating.

To avoid spalling completely the uniaxial compressive strength would have to be about 170 MPa even assuming the 55% threshold and the lower bound stress estimate given in the site reports (Table 2-2). This is about 40–60% higher than the minimum uniaxial strength values given for the foliated Olkiluoto gneiss. In summary: using less conservative values as input to the evaluation of the results obtained would not change the overall conclusions.

References

- Cho N, Martin C D, Christiansson R, 2002.** Suppressing fracture growth around underground openings. In Proc. 5th North American Rock Mechanics Symposium and 17th Tunnelling Association of Canada Conference NARMS/TAC 2002, Toronto (Ed. Hammah R, Baden W, Curran J, Telesnicki M), vol. 2, pp 1151–1158, University of Toronto Press, Canada.
- Claesson J, Probert T, 1996a.** Temperature field due to a large rectangular grid source. Derivation of an analytical solution. SKB TR-96-12, Svensk Kärnbränslehantering AB, Sweden.
- Claesson J, Probert T, 1996b.** Thermoelastic stress due to a rectangular heat source in a semi-infinite medium. Derivation of an analytical solution. SKB TR-96-13, Svensk Kärnbränslehantering AB, Sweden.
- Hökmark H, Fälth B, 2003.** Thermal dimensioning of the deep repository. Influence of canister spacing, canister power, rock thermal properties and nearfield design on the maximum canister surface temperature. SKB TR-03-09, Svensk Kärnbränslehantering AB, Sweden.
- Hökmark H, Fälth B, Wallroth T, 2006.** THM couplings in rock. Overview of results of importance to the SR-Can safety assessment. SKB R-06-88, Svensk Kärnbränslehantering AB, Sweden.
- Ikonen K, 2003.** Thermal Analyses of Spent Nuclear Fuel Repository. Report POSIVA 2003-04. Posiva Oy, Olkiluoto, Finland.
- Itasca, 2003.** *3DEC* – 3-Dimensional Distinct Element Code, User’s Guide. Itasca Consulting Group, Inc. Minneapolis, USA.
- Kalbanter P, Johannesson L-E, 2000.** Hållfasthetsberäkningar för en bentonitbuffert bestående av enaxligt kompakterade bentonitkroppar. SKB R-00-42, Svensk Kärnbränslehantering AB, Sweden.
- Kirsch G, 1898.** Die Theorie der Elastizität und die Bedürfnisse der Festigkeitslehre. Zeit. Ver. Deut. Ing. 42, 797–807.
- Martin D, 2005.** Preliminary assessment of potential underground stability (wedge and spalling) at Formark, Simpevarp and Laxemar sites. SKB R-05-71, Svensk Kärnbränslehantering AB, Sweden.
- Paananen M, Paulamäki P, Gehör S, Kärki A, Front K, Aaltonen I, Ahokas T, Kemppainen K, Mattila J, Wikström L, 2006.** Geological Model of the ONKALO Area Version 0. Working Report 2006-13. Posiva Oy, Olkiluoto, Finland.
- Paulamäki S, Paananen M, Gehör S, Kärki A, Front K, Aaltonen I, Ahokas T, Kemppainen K, Mattila J, Wikström L, 2006.** Geological Model of the Olkiluoto Site Version 0. Working Report 2006-37. Posiva Oy, Olkiluoto, Finland.
- Posiva, 2005.** Olkiluoto Site Description 2004. Report POSIVA 2005-03. Posiva Oy, Olkiluoto, Finland.
- Posiva, 2006.** Nuclear Waste Management of the Olkiluoto and Loviisa Power Plants: Programme for Research, Development and Technical Design for 2007–2009. TKS-2006. Posiva Oy, Olkiluoto, Finland.
- Posiva, 2007.** Olkiluoto Site Description 2006. Report POSIVA 2007-03. Posiva Oy, Olkiluoto, Finland.

Probert T, Claesson J, 1997. Thermoelastic stress due to a rectangular heat source in a semi-infinite medium. Application for the KBS-3 repository. SKB TR-97-26, Svensk Kärnbränslehantering AB, Sweden.

SKB, 2005. Preliminary site description. Forsmark area – version 1.2. SKB R-05-18, Svensk Kärnbränslehantering AB, Sweden.

SKB, 2006a. Preliminary site description. Laxemar subarea – version 1.2. SKB R-06-10, Svensk Kärnbränslehantering AB, Sweden.

SKB, 2006b. Long-term safety for KBS-3 repositories at Forsmark and Laxemar – a first evaluation- Main report of the SR-Can project. SKB TR-06-09, Svensk Kärnbränslehantering AB, Sweden.

Timoshenko S P, Goodier J N, 1970. Theory of Elasticity. 3rd Edition. Wiley, New York, USA.

Revision of Olkiluoto KBS-3H lay-out adaptation

A1.1 Introduction

The bedrock factors affecting the KBS-3H lay-out were presented in Posiva working report 2002-57 /Johansson et al. 2002/ and they were further evaluated in 2005 to define the future need for updating (S&R memorandum PM KBS-3H Safety Case 12-2005, Project 756-106). The results of the evaluation indicated that, in general, only insignificant changes have occurred since 2002 in the Olkiluoto site-specific hydrogeological, (geological), rock mechanical and thermal property conditions. However, there have been changes in the amount of spent fuel, which affects the repository size, new information on the distribution of hydraulic leakages, inflow acceptance criteria and a novel principle of dividing the drifts into compartments.

Hence a study was made to adapt the KBS-3H lay-out to the Olkiluoto site specific conditions. The work is a kind of an update of the previous KBS-3H adaptation (Posiva Working Report 2002-57) but it applies also the experiences used in the KBS-3V adaptation exercise (Posiva Working Report 2003-68).

A1.2 Present Olkiluoto KBS-3V lay-out adaptation

Olkiluoto KBS-3V lay-out adaptation was presented in /Malmlund et al. 2003/ (Posiva Working Report 2003-68). The examples presented for a KBS-3V type repository were either in one or two layers. The examples considered the latest developments in the repository layout design work, the ONKALO draft designs, an increase of 50% in the amount of waste due to the decision of a new reactor OL3 (total number of canisters was 3,000), an increase in the canister spacings due to changes in the thermal dimensioning of the repository, an alternative 40 m deposition tunnel spacing in addition to the original 25 m spacing, updating of the bedrock model (model 2003/1) and a proposal for a new host rock classification system (HRC-system). Two canister spacings were used in the case of 25 m deposition tunnel spacing – 11 m for TVO fuel and 8.6 m for Fortum fuel (about 700 canisters).

The design bases used in the adaptation work were updated and the various requirements set for the repository were considered in terms of locating the above-ground facilities, selecting a suitable depth range for the repository, locating the repository horizontally (in particular, with respect to fracture zones) and orienting the deposition tunnels as favourably as possible.

The comparison of the two deposition tunnel spacings revealed that the 25 m spacing was more efficient in terms of resource utilisation than the 40 m spacing. The 40 m tunnel spacing was, however, more cost efficient, since the canisters can be disposed more densely in the deposition tunnels, resulting in a reduction of some 20–25% in the total length of deposition tunnels to be excavated and filled.

In four KBS-3V examples a number of imaginary structures were considered in addition to the structures of the bedrock model. The imaginary structures, representing the yet unidentified structures of the bedrock, resulted in a general shortening of individual deposition tunnels as the bedrock resources split into smaller bedrock blocks, as well as an extending of the central tunnels.

/Malmlund et al. 2003/ evaluated that 17% of the canister locations within the disposal area at Olkiluoto would be unsuitable (due to the conductive sections and poor rock quality) based on the HRC-system.

In one storey concept, level –420 m and including the imaginary structures, the utilization degree of the site was 79% (1.5 km²/1.9 km²).

A1.3 Application of HRC and respect distances

A Host Rock Classification (HRC) system has been developed for the Olkiluoto site for identifying suitable volumes of rock for the disposal of spent nuclear fuel /Hagros et al. 2005/. The HRC-system is, however, specific to the KBS-3V disposal concept and is not directly applicable to the KBS-3H concept, although it may well be that the host rock defined as suitable for a KBS-3V repository is equally suitable for a KBS-3H repository. It is outside the scope of this preliminary work to study this possible equivalence in any detail and instead, the HRC-system will be used only where necessary, *i.e.* in defining the respect distances to layout-determining fracture zones, and with only minimal modifications. The respect distances to Class A and B fracture zones are shown in Table 1, where the horizontal deposition drifts are assumed to correspond to the deposition tunnels of the KBS-3V system and similar respect distances will be used. The same classification of fracture zones at Olkiluoto will be used as was presented in the layout adaptation work for the KBS-3V system /Malmlund et al. 2003/.

Other parameters of the HRC-system will not be considered in this preliminary work.

A1.4 Effect of geohydrological conditions

Transmissive sections were estimated based on the work by /Hellä et al. 2006/ (in print). Three inflow classes as shown in Table 2 were used. The calculation of the transmissive sections in the repository that require compartment plugs or bentonite blocks is presented in Table 3. Data from the hydraulic measurements carried out in boreholes KR1...KR23 (depth interval 350–570 m) were used, whenever available (these boreholes were chosen because they were considered in the bedrock model 2003/1 that was used here). The calculations indicate that 21% of the bedrock resource is unusable due to too high transmissivities ($> 2.65E-09$ m²/s) and the related need of compartment plugs and bentonite blocks. This value was decided to be tentatively rounded up to 30% to include the probable effect of other factors (e.g. low rock quality and non-transmissive Class C fracture zones).

A1.5 Input data table

It is assumed that the repository will be constructed in one layer at about –400 m depth at Olkiluoto. The total amount of fuel is based on the present estimate, which corresponds to 3,000 canisters. Similar requirements and bases are used as in the present KBS-3V adaptation to produce comparable result. Due to the unusable bedrock resource (30%) as shown in Table 4, a space for 4,290 canisters would be needed.

Table A1-1. Layout-determining fracture zones (Class A and B) and the related respect distances (modified from /Hagros et al. 2005/). In the KBS-3H design it is assumed that the deposition drift corresponds to the deposition tunnel in the KBS-3V concept.

Class	Fracture zones in the class	Basis for the definition of fracture zone class		Respect distance
A	Fracture zones that cannot be intersected by any part of the repository below a depth of 300 m.	A1	Length $\geq 5,000$ m	1% of the length, 100 m at most
		A2	$T_{400m} \geq 1E-05$ m ² /s	50 m
B	Fracture zones that cannot be intersected by deposition drifts but can be intersected by other parts of the repository.	B1	$1E-06 \leq T_{400m} < 1E-05$ m ² /s	40 m
		B2	$1E-07 \leq T_{400m} < 1E-06$ m ² /s	30 m
		B3	$Q' < 0.5$ and thickness ≥ 5 m	15 m

Table A1-2. Inflow classes (related to transmissivity) of rock mass within the bedrock resource and their effects on the locating of canisters in KBS-3H deposition drifts.

Inflow (l/min) into one supercontainer section from fractures without sealing	Transmissivity (m ² /s) assuming one inflowing fracture ¹⁾	Effect on the locating of canisters (KBS-3H supercontainers) and the need for seals (isolation)
Inflow < 0.1	T < 2.65E-9	No effect (a supercontainer can be located into the section)
0.1 ≤ Inflow < 1	2.65E-9 ≤ T < 2.65E-8	A bentonite block of 10 m shall be located into the section.
Inflow ≥ 1	T ≥ 2.65E-8 ²⁾	A compartment plug unit of 30 m ³⁾ in total shall be located into the section.

1) Transmissivity calculated from inflow using the Thiem equation and assuming a constant head of 400 m at a radius of 50 m from the tunnel (radius 0.925 m).

2) If T ≥ 1E-7 m²/s, the section probably belongs to a Class A or B fracture zone (see Table 1) and such sections should, therefore, not occur in the bedrock resource where the deposition drifts are located.

3) 30 m = stabilization zone 10 m + fracture zone (conductive section) 10 m + stabilization zone 10 m.

Table A1-3. Calculation of the percentage of transmissive sections (that require compartment plugs or bentonite blocks, see Table 2) at Olkiluoto. Borehole data from the depth range 350–570 m (vertical depth below sea level) have been used. Transmissivities were evaluated from the borehole flow measurement data measurements /Pöllänen and Rouhiainen 1996a, 1996b, 1997, 2000, 2002, Rouhiainen 2000, Pöllänen et al. 2005/.

Rock mass outside Class A and B respect zones ¹⁾

Borehole	Borehole data	The number of sections T > 2.65E-08 m ² /s	The number of sections T = 2.65E-09...2.65E-08 m ² /s	Compartment plug sections ²⁾	Bentonite block sections ³⁾	Usable rock mass (outside blocks and plugs)
	length	nos.	nos.	m	m	m
KR01	8	0	1	0	8	0
KR02	190	0	1	0	10	180
KR03	54	0	4	0	40	14
KR04	230	1	4	30	26	174
KR06	86	0	1	0	10	76
KR07	236	0	1	0	10	226
KR08	52	0	1	0	10	42
KR09	112	1	2	30	20	62
KR10	222	1	4	30	40	152
KR11	204	0	1	0	10	194
KR12	226	0	4	0	40	186
KR14	126	1	1	30	10	86
KR19	72	0	3	0	30	42
KR22	40	0	0	0	0	40
Σ	1858			120	264	1474
%	100 %			6.5 %	14.2 %	79.3 %

1) In addition to the actual fracture zone intersections, the nearest 30 m from both above and below the fracture zone intersection were excluded representing the respect distance

2) Total length of sections requiring a 30 m compartment plug (possible overlapping of transmissive sections and ending of data range are taken into account)

3) Total length of sections requiring a 10 m bentonite block (possible overlapping of transmissive sections and ending of data range are taken into account)

(Transmissive sections were identified from the borehole data by using limits for K_{2m} of 1.33E-08 and 1.33E-09 m/s. When several transmissive 2 m sections were within 10 meters, the total transmissivity of these 10 m sections were calculated and used in the analysis.)

Table A1-4. Input data for Olkiluoto KBS-3H adaptation.

Parameter	Value/criterion
Number of canisters	3,000
Repository concept	KBS-3H, one layer, no side tunnels – other parts than deposition drifts and related niches are similar to present KBS-3V design
Bedrock model	Olkiluoto 2003/1 model
Bedrock resource	As in WR 2003-68 + imaginary structures* + 30% of resource considered unusable**
Respect distances	As in Table 1
Depth level	400 m***
Spacing between deposition drifts (Canister length)	25 m*** 4,835 mm)
Canister spacing (center to center distance) (Supercontainer length (Distance block length Length of deposition drift Orientation of deposition drift Other space requirements	10.9 m *** 5,560 mm***) 5,350 mm***) 100 – 300 m*** 120 ± 10° (parallel to the assumed main principal stress)**** First canister 25 m from the central tunnel

* Taken as in WR 2003-68 (Class B fracture zones, see Table 1).

** 21% of the bedrock resource is unusable due to too high transmissivities ($> 2.65E-09$ m²/s) and the related need of compartment plugs and bentonite blocks (see Tables 2 and 3). This value is tentatively rounded up to 30% to include the probable effect of other factors (e.g. low rock quality and non-transmissive Class C fracture zones) on the locating of the canisters (cf. WR 2003-68). In the adaptation work, this 30% unusability of resource is considered by increasing the number of canisters by 43% ($= 30/(100-30)$) to 4,290 canisters.

*** Input parameters for Safety-Case (S&R Memo 756-11/2005 PM Input parameters for HMCGB analyses, version 6.12.2005).

**** As in WR-2002-57.

A1.6 KBS-3H lay-out adaptation example

The input data shown in Table 4 were used to adapt the KBS-3H lay-out to the Olkiluoto site. The “best” realization is shown in Figure 1. In this example there are 156 canister drifts, the average canister drift length is 264 m and the total canister drift length is 41,167 m. There are 3,419 canister locations in the lay-out example, which is 79.7% of the target number, *i.e.* 4,290.

When using the above described input assumptions, the utilization degree of the Olkiluoto site is then about 120% in the KBS-3H concept, whereas it was about 80% in the KBS-3V concept. It should be noted that in the KBS-3V adaptation canister spacing 8.6 m was used for Fortum’s 700 canisters. This effect is, however, considered to be small.

A1.7 Conclusion

Using the input data described in Table 4 there is not enough available bedrock resource to adapt the KBS-3H concept in one layer. Coming updates (during 2006) of geological and geohydrological site model will in more detail show the usable bedrock resources.

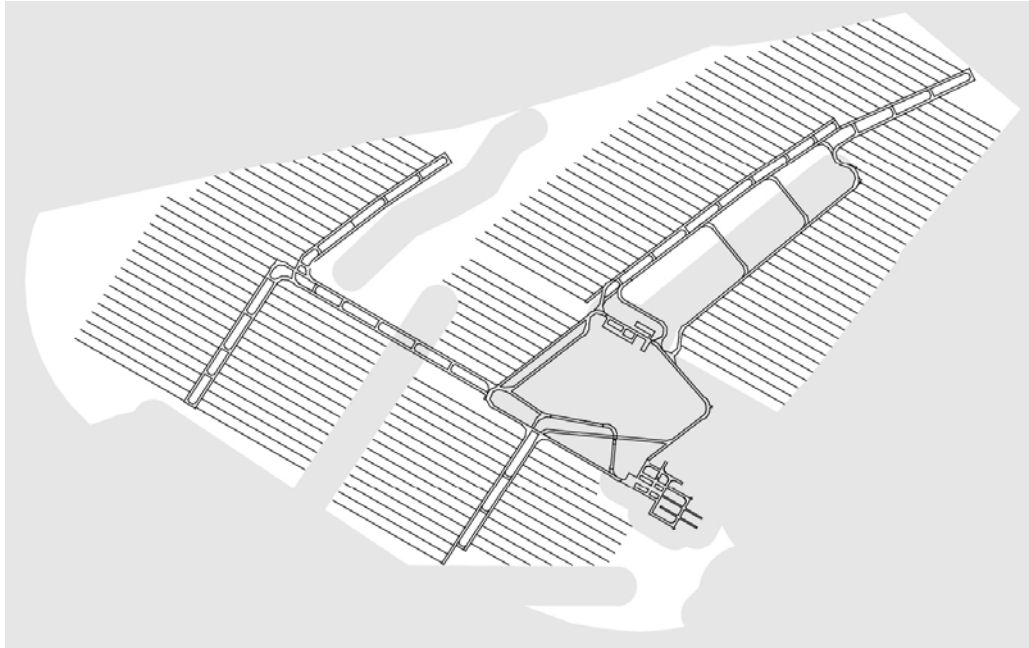


Figure A1-1. KBS-3H lay-out adaptation to the Olkiluoto site, depth level 400 m. White areas indicate the usable bedrock resource.

References

- Hagros A, McEwen T, Anttila P, Äikäs K, 2005.** Host Rock Classification Phase 3: Proposed Classification System (HRC-System). Olkiluoto, Finland: Posiva Oy. Working Report 2005-07.
- Hellä P, Ahokas H, Palmén J, Tammisto E, 2006.** Analysis of geohydrological data for design of KBS-3H repository lay-out. Olkiluoto, Finland: Posiva Oy. Posiva Working Report 2006-16.
- Johansson E, Äikäs K, Autio J, Hagros A, Malmlund H, Rautakorpi J, Sievänen U, Wanne T, Anttila P, Raiko H, 2002.** Preliminary KBS-3H layout adaptation for the Olkiluoto site. Analysis of rock factors affecting the orientation of a KBS-3H deposition hole. Olkiluoto, Finland: Posiva Oy. Working Report 2002-57.
- Malmlund H, Äikäs K, Hagros A, 2003.** Layout adaptation examples for a KBS-3V repository at Olkiluoto. Olkiluoto, Finland: Posiva Oy. Working Report 2003-68.
- Pöllänen J, Rouhiainen P, 1996a.** Difference flow measurements at the Olkiluoto Site in Eurajoki, boreholes KR1-KR4, KR7 and KR8. Helsinki, Finland: Posiva Oy. Work Report PATU-96-43e.
- Pöllänen J, Rouhiainen P, 1996b.** Difference flow measurements at the Olkiluoto site in Eurajoki, boreholes KR9 and KR10. Helsinki, Finland: Posiva Oy. Work Report PATU-96-44e.
- Pöllänen J, Rouhiainen P, 1997.** Groundwater flow measurements at the Olkiluoto site in Eurajoki, boreholes KR1-KR4 and KR7-KR9. Olkiluoto, Finland: Posiva Oy. Working Report 97-27e.
- Pöllänen J, Rouhiainen P, 2000.** Difference flow and electric conductivity measurements at the Olkiluoto site in Eurajoki, boreholes KR6, KR7 and KR12. Olkiluoto, Finland: Posiva Oy. Working Report 2000-51.
- Pöllänen J, Rouhiainen P, 2002.** Difference flow and electric conductivity measurements at the Olkiluoto site in Eurajoki, boreholes KR13 and KR14. Olkiluoto, Finland: Posiva Oy. Working Report 2001-42.

Pöllänen J, Pekkanen J, Rouhiainen P, 2005. Difference flow and electric conductivity measurements at the Olkiluoto site in Eurajoki, boreholes KR19-KR28, KR19B, KR20B, KR22B, KR23B, KR27B and KR28B. Olkiluoto, Finland: Posiva Oy. Working Report 2005-52.

Rouhiainen P, 2000. TDS measurements and detailed flow logging at the Olkiluoto site in Eurajoki, boreholes KR1-KR11. Helsinki, Finland: Posiva Oy. Working Report 99-72.

List of input parameters for KBS-3H process report and evolution report

A list of input parameters to be used in the HMCGB analyses of steel components has been defined in the Appendix A of the report by /Johnson et al. 2005/ HMCGB processes related to the steel components in the KBS-3H disposal concept, Posiva Working Report 2005-09.

These parameters have been checked and updated for the KBS-3H Process Report and Evolution Report.

As the design has changed since the list of input parameters was compiled in June 2004, the checking of parameters has been done on all of those parameters, which are independent of the design options. The materials and dimensions for the new design options BD and DAWE will be compiled in 2006 as soon the design is on a more mature stage.

The data has been reviewed and checked by Jorma Autio, Lennart Börgesson, Bo Halvarsson and Margit Snellman.

APPENDIX A List of input parameters

Parameter	Unit	Symbol	Reference value	Alternative values	Comment/ Ref.
System Description					
Repository depth					
one-storey	m		400	420	/Johnson et al. 2005/
two-storeys	m			400 and 500	/Johnson et al. 2005/
Deposition drift					
diameter	mm	$2 r_t$	1,850	1,840	/Börgesson et al. 2005/
length	m		300		/Johnson et al. 2005/
separation between drifts	m	d	25	40	/Johnson et al. 2005/
drift dip	°		2 +/-1		Meeting 28.05.04
drift orientation	–		parallel to max. stress		/Johnson et al. 2005/
Canister					
outer diameter	m	$2 r_c$	1.05		/Börgesson et al. 2005/
length	m	l_c	4.835		/Autio et al. 2007/
pitch (center-to-center distance)	m	p_c	11.0	7.30 – 7.95, SKB	(Posiva BWR 1,700 W)
	m		9.1	BWR 8.6 (SKB)	(Posiva VVER 1,370 W)
	m		10.6(Posiva)	8.1 (SKB)	Posiva EPR 1,830 W)
/Johnson et al. 2005/					
Supercontainer (perforated)					
total mass	kg		[850 kg, 890 kg with feet]		
length	mm	l_{sc}	5,560 +5/0		
feet	kg		40.2		/Autio et al. 2007/
outer diameter	mm	$2 r_{sc}$	1,765		/Börgesson et al. 2005/
inner diameter	mm		1,749		/Börgesson et al. 2005/
thickness (of end plates)	mm		8		/Börgesson et al. 2005/
radius of perforation holes	mm		100		/Börgesson et al. 2005, Blix 2004/
degree of perforation	%		62		/Börgesson et al. 2005, Blix 2004/

Parameter	Unit	Symbol	Reference value	Alternative values	Comment/ Ref.
Distance blocks					
diameter	mm		1,765	1,845	/Börgesson et al. 2005/
length (depending on drift sep.)	mm		5,465 (Posiva 25m)	1.73–2.38 (SKB 40m)	OL 1-2, Posiva BWR 1,700 W, SKB BWR 1,700W /Autio et al. 2007/
			4,765 (25m)	2,550 (40m)	Posiva VVER 1370. /Autio et al. 2007/
void slot (option DAWE)	mm		37.5–42.5		/Börgesson et al. 2005/
Supporting feet, 4 feet per block, total mass	kg		13.9		/Autio et al. 2007/
void slot (Basic Design)	mm		2–20		Design description 2006 /Autio et al. 2007/
Bentonite blocks					
initial water content	w-%		10	20	/Börgesson et al. 2005/ Design description 2006 /Autio et al. 2007/
saturated density after swelling	kg m ⁻³		2,000		/Börgesson et al. 2005/
saturated porosity after swelling	%	ϵ_b	44	(for 20% = ?)	SKB TR 99-07
swelling pressure	MPa		7–8	8.7 in SKB TR 99-07	Meeting 28.05.04
gap to canister (radial)	mm		5		/Börgesson et al. 2005/
gap to super container (radial)	mm		5		
diameter end blocks	mm		1,740		/Autio et al. 2007/
diameter ring blocks	mm		1,740		/Autio et al. 2007/
length end blocks	mm		350		/Börgesson et al. 2005/
length ring blocks	mm		4,844 (4*1,211)		/Autio et al. 2007/
(Bentonite pellets) No pellets					
initial water content	w-%		10		/Börgesson et al. 2005/
initial density	kg m ⁻³		1,000		/Börgesson et al. 2005/
dry density	kg m ⁻³		909		/Börgesson et al. 2005/
Supporting feet (supercontainer)					
material type	–		steel		
total mass (per canister)	kg		40.2		10 feet per supercontainer
Supporting feet (distance block, DAWE)					
material type	–		steel		
total mass (per canister)	kg		13.9		4 feet per distance block
Fixing ring to prevent movement of distance block (BD)					
material type	–		10 mm thick steel plate		
total mass	kg		600	1,200	/Autio 2007/
Fixing material, cement	l		15		Low pH cement. Estimate based on 10 cm deep and 20 cm wide groove.
Steel compartment plug					
material type, steel	–		10 mm steel plate		
total mass	kg		2,110		KBS-3H /Autio et al. 2007/
fixing material, cement	l		190		/Autio et al. 2007/
Drift end plug	m ³		12	1.2	Short wedge shaped plug and rock kernel plug.

Parameter	Unit	Symbol	Reference value	Alternative values	Comment/ Ref.
Filling blocks					Present assumption: similar to distance blocks.
Spray and drip shield					
BD and DAWE	kg		0.6		Design description 2005. One unit, based on demonstration shield at Äspö.
Drainage, artificial wetting and air evacuation pipes (DAWE)					10 mm diameter air pipe, 17.2 mm diameter wetting pipes. Paul-Erik Rönnqvist will provide more exact data on the masses.
Grouting material per drift					Being evaluated, present estimate 5 l of grout per leaking fracture of aperture 50 microns.
Low-pH cement	kg				
Silica Sol	kg				
Grouting material per supercontainer unit (SC+DB)	kg				
Low-pH cement	kg				Other stray materials
Silica Sol					/Hagros 2007/
Other stray materials per drift					
Nitrogen compounds	kg				
Organics (oil etc)	kg				
Geochemical and biological conditions					
Host rock chemistry					
Salinity	g l ⁻¹		10–25	25–45	/Posiva 2003, Johnson et al. 2005/
Alkalinity	meq l ⁻¹		0.4	0.1–1	/Posiva 2003/
pH			7.5–8.2		/Posiva 2003/
Redox potential	mV		–300–250	≈ –200	/Posiva 2003, Pitkänen et al. 2004/
Redox conditions			methanogenic	sulphidic	/Posiva 2003/
Degradable organic matter (n.a)	% rock		0		Meeting 28.05.04
Dissolved Fe(II)	mg l ⁻¹		0.07	0–0.5	/Pitkänen et al. 2004/
Dissolved sulphide			0–3	12 (max)	/Posiva 2005/ (site report)
Dissolved gases					
H ₂	ml l ⁻¹		< 0.1 generally	7–268 (a max.value below 800 m)	Not near saturation /Gascoyne 2000, Pitkänen et al. 2004/
CH ₄	ml l ⁻¹		< 400 generally at depths down to 500 m	770–990 (max.values below 800 m)	Near sat.in saline water < 800 m, /Gascoyne 2000, Pitkänen et al. 2004/
Solubilities at 30°C (after. approx. 2000a TR99-07 p. 100) and 0.1 MPa					
H ₂	ml l ⁻¹		0.77 19		/Himmelblau 1960/
CH ₄	mol m ⁻³ ml l ⁻¹		1.3 33		/Himmelblau 1960/
Bentonite					
Bentonite type			MX-80		TILA-99 /Vieno and Nordman 1999/
Porewater composition					
Fe(II) mineral content (pyrite, siderite)	%		1	0	/Müller-Vonmoos 1983/
Steel corrosion rate	µm a ⁻¹ R		1	2 1–2	/Smart et al. 2004/ Sensitivity anal.

Parameter	Unit	Symbol	Reference value	Alternative values	Comment/ Ref.
Rock properties					
Gneiss: fracture properties					
fracture type	–		fractures	vein-like	Sparsely fractured rock and occasional “vein-like sections” /Johnson et al. 2005/ see also /Posiva 2003/ and note at the end of this paper.
orientation	–		several sets		
density	m ⁻³	N	1–3	3–10	
aperture	mm	a	calc. from T-distribution		
transmissivity	m ² s ⁻¹	T	10 ⁻¹⁴ –10 ⁻⁷		
hydraulic conductivity	m s ⁻¹		10 ⁻⁸ – 10 ⁻¹⁵		/Börgesson et al. 2005/
Gneiss: average matrix properties					
porosity	%	ε _m	0.14	0.1–0.2	/Johnson et al. 2005*/
hydraulic conductivity	m s ⁻¹		1E-14	≈< 1E-15	/Hautajärvi 2004/
gas effective diffusion constant	m ² s ⁻¹		2.63E-10		/Johnson et al. 2005/
intrinsic gas permeability	m ²		5.16E-21		/Johnson et al. 2005/
EDZ: properties of crushed zone (0–4 mm)					
thickness (radial extent)	mm		4		/Johnson et al. 2005/
porosity	%		0.64	2–4	/Johnson et al. 2005/
fracture type	–		open cracks		/Johnson et al. 2005/
Hydraulic properties?					
mean fracture aperture	μm		2		/Johnson et al. 2005/
small fractures (< 5.4 μm)	%		90		/Johnson et al. 2005/
larger fractures (> 5.4 μm)	%		10		/Johnson et al. 2005/
EDZ: properties of microfractured zone (4–9 mm)					
thickness (radial extent)	mm		5		/Johnson et al. 2005/
porosity	%		0.34		/Johnson et al. 2005/
fracture type	–		open cracks		/Johnson et al. 2005/
Hydraulic properties?					
mean crack specific surface	μm ⁻¹		0.004		/Johnson et al. 2005/
small fractures (< 2.16 μm)	%		60%		/Johnson et al. 2005/
EDZ: properties of zone of minor damage (9–23 mm)					
Thickness (radial extent)	mm		14		/Johnson et al. 2005/
Fracturation	–		similar as in undisturbed rock		/Johnson et al. 2005/
EDZ: average properties (0–23 mm)					
porosity	%	ε _{EDZ}	0.34		/Johnson et al. 2005/
Hydraulic properties?					
gas effective diffusion constant	m ² s ⁻¹		3.97E-9		/Johnson et al. 2005**/
intrinsic gas permeability	m ²		2.96E-19		/Johnson et al. 2005***/
Hydraulic properties of rock					
Leakage rates for 300 m drift (operational phase)	litres• .min ⁻¹				/Johnson et al. 2005// Hellä et al. 2006/
long dry sections			“dry”		
1–3 local fracture zones			> 4 (one per 250 m)		Range of inflow from local fracture zones

Parameter	Unit	Symbol	Reference value	Alternative values	Comment/ Ref.
A few fractures or fracture zones (per 100 m)			0.4–4 (one per 100 m)		
Six 5 m long sections (per 300 m)			> 0.1		
Four to five 10 m long sections(per 300 m)			> 0.1		
Total leakage per compartment			10 (total)		e-mail MS 5.11.05 On the average four transmissive fractures (> 0.01l/min) per 100 m sample length
Total leakage per drift			30 (total)		e-mail MS 5.11.05
Saturation time	a		10	12,000	Meeting 28.05.04
Hydraulic gradient (post-closure phase)	m m ⁻¹		0.01		/Johnson et al. 2005/
Thermal properties of rock					
Ambient temperature	°C	T ₀	+10.5°C (400m)		/Ikonen 2003/, gradient 1.5°C / 100 m
Heat output	W				/Johnson et al. 2005/
BWR canister			1,700		
PWR canister			1,370		
Thermal conductivity (gneiss)	Wm ⁻¹ K ⁻¹		2.7		/Posiva 2003/, p. 114
Heat capacity (gneiss)	J kg ⁻¹ K ⁻¹		797		/Posiva 2003/, p. 114
Thermal diffusivity (gneiss)	m ² s ⁻¹		1.23E-06		/Posiva 2003/, p. 114
Thermal conductivity (bentonite)	Wm ⁻¹ K ⁻¹		1.0		/Johnson et al. 2005/
Maximum temperature at canister surface (for thermal dimensioning)	°C		90		10° below the design basis max. of 100° /Johnson et al. 2005/

* These values represent Gneissic tonalite in the Research Tunnel at Olkiluoto.

** Scaling factor to convert to diffusivity of heavier molecules in water saturated samples by 1/35,000 /Autio et al. 1999/.

*** Hydraulic conductivity can be calculated using permeability /e.g. Autio et al. 1999/.

References for Table A-1:

Autio J, 2004. Description of excavation damaged zone (EDZ) around a KBS-3H deposition drift, PM KBS-3H Safety case 10/2004, Saanio & Riekkola Oy, Helsinki.

Autio J, 2007. KBS-3H design description 2005. Working Report 2007-11 and SKB R-08-29. Posiva Oy, Olkiluoto, Finland and Svensk Kärnbränslehantering AB, Sweden.

Autio J, Börgesson L, Sandén T, Rönnqvist P-E, Johansson E, Hagros A, Eriksson M, Berghäll J, Kotola R, Parkkinen I, 2007. KBS-3H design description 2006. Working Report 2007-105 and SKB R-08-32. Posiva Oy, Olkiluoto, Finland and Svensk Kärnbränslehantering AB, Sweden.

Autio J, Kirkkomäki T, Siitari-Kauppi M, Timonen J, Laajalahti M, Aaltonen T, Maaranen J, 1999. Use of 14C-PMMA method and He-gas methods to characterize excavation disturbance in crystalline rock. POSIVA 99-22, Posiva Oy, Helsinki.

Blix P, 2004. Sweco PIC, SKB KBS-3H finite element analysis of supercontainer, (15. Nov. 2004): (Found at Projectplace).

- Börgesson L, Sandén T, Fälth B, Åkesson M, Hökmark H, 2005.** Behaviour of the buffer in KBS-3H, SKB-TR-05-50. Svensk Kärnbränslehantering AB, Sweden.
- Gascoyne M, 2000.** Dissolved gases in groundwaters at Olkiluoto. Working Report 2000-49. Posiva Oy, Helsinki.
- Hagros A, 2007.** Estimated quantities of residual material in a KBS-3H repository at Olkiluoto. Posiva Working Report 2007-104 and SKB R-08-33. Posiva Oy, Olkiluoto, Finland and Svensk Kärnbränslehantering AB, Sweden.
- Hautojärvi A, 2004.** Interview by Ari Ikonen, June 15, 2004.
- Hellä P, Ahokas H, Palmén J, Tammisto E, 2006.** Analysis of geohydrological data for assessment of the alternative repository layout KBS-3H. Working Report 2006-16. Posiva Oy, Olkiluoto.
- Himmelblau D M, 1960.** Solubilities of inert gases in water. J. Chem. Eng, Vol. 5/1, January 1960.
- Ikonen K, 2003.** Thermal Analyses of KBS-3H Type repository. POSIVA 2003-11, Posiva Oy, Olkiluoto.
- Johnson L, Marschall P, Wersin P, Gribi P, 2005.** HMCSBG processes related to the steel components in the KBS-3H disposal concept. Working Report 2005-09. Posiva Oy, Olkiluoto.
- Müller-Vonmoos M, Kahr G, 1983.** Mineralogische Untersuchungen von Wyoming Bentonite MX-80 und Montigel. Nagra Technical Report NTB 83-12, Nagra, Wettingen, Switzerland.
- Pitkänen P, Partamies S, Luukkonen A, 2004.** Hydrogeochemical interpretation of baseline groundwater conditions at the Olkiluoto site. POSIVA 2003-07, Posiva Oy, Olkiluoto.
- Posiva, 2003.** Baseline conditions at Olkiluoto. POSIVA 2003-02, Posiva Oy, Olkiluoto.
- Posiva, 2005.** Olkiluoto site description 2004. Report POSIVA 2005-03. Posiva Oy, Olkiluoto, Finland.
- Smart N R, Rance A P, Werme L O, 2004.** Anaerobic corrosion of steel in bentonite – Mat. Res. Soc. Symp. Proc. 807, 441–446.
- Vieno T, Nordman H, 1999.** Safety assessment of spent fuel disposal in Hästholmen, Kivetty, Olkiluoto and Romuvaara TILA-99. POSIVA 99-07. Posiva Oy, Helsinki, Finland.
- Vuorinen U, Kulmala S, Hakanen M, Ahonen L, Carlsson T, 1998.** Solubility database for TILA –99. POSIVA 98-14, Posiva Oy, Helsinki.